EUROPEAN LABORATORY FOR PARTICLE PHYSICS

Tests of the Standard Model and Constraints on New Physics from Measurements of Fermion-pair Production at 189 GeV at LEP

The OPAL Collaboration

Abstract

Cross-sections and angular distributions for hadronic and lepton pair final states in e^+e^- collisions at a centre-of-mass energy near 189 GeV, measured with the OPAL detector at LEP, are presented and compared with the predictions of the Standard Model. The results are used to measure the energy dependence of the electromagnetic coupling constant α_{em}, and to place limits on new physics as described by four-fermion contact interactions or by the exchange of a new heavy particle such as a sneutrino in supersymmetric theories with R-parity violation. A search for the indirect effects of the gravitational interaction in extra dimensions on the $\mu^+\mu^-$ and $\tau^+\tau^-$ final states is also presented.

The OPAL Collaboration

G. Abbiendi[2], K. Ackerstaff[8], G. Alexander[23], J. Allison[16], K.J. Anderson[9], S. Anderson[12], S. Arcelli[17], S. Asai[24], S.F. Ashby[1], D. Axen[29], G. Azuelos[18,a], A.H. Ball[8], E. Barberio[8], R.J. Barlow[16], J.R. Batley[5], S. Baumann[3], J. Bechtluft[14], T. Behnke[27], K.W. Bell[20], G. Bella[23], A. Bellerive[9], S. Bentvelsen[8], S. Bethke[14], S. Betts[15], O. Biebel[14], A. Biguzzi[5], I.J. Bloodworth[1], P. Bock[11], J. Böhme[14], O. Boeriu[10], D. Bonacorsi[2], M. Boutemeur[33], S. Braibant[8], P. Bright-Thomas[1], L. Brigliadori[2], R.M. Brown[20], H.J. Burckhart[8], P. Capiluppi[2], R.K. Carnegie[6], A.A. Carter[13], J.R. Carter[5], C.Y. Chang[17], D.G. Charlton[1,b], D. Chrisman[4], C. Ciocca[2], P.E.L. Clarke[15], E. Clay[15], I. Cohen[23], J.E. Conboy[15], O.C. Cooke[8], J. Couchman[15], C. Couyoumtzelis[13], R.L. Coxe[9], M. Cuffiani[2], S. Dado[22], G.M. Dallavalle[2], S. Dallison[16], R. Davis[30], S. De Jong[12], A. de Roeck[8], P. Dervan[15], K. Desch[27], B. Dienes[32,h], M.S. Dixit[7], M. Donkers[6], J. Dubbert[33], E. Duchovni[26], G. Duckeck[33], I.P. Duerdoth[16], P.G. Estabrooks[6], E. Etzion[23], F. Fabbri[2], A. Fanfani[2], M. Fanti[2], A.A. Faust[30], L. Feld[10], P. Ferrari[12], F. Fiedler[27], M. Fierro[2], I. Fleck[10], A. Frey[8], A. Fürtjes[8], D.I. Futyan[16], P. Gagnon[7], J.W. Gary[4], G. Gaycken[27], C. Geich-Gimbel[3], G. Giacomelli[2], P. Giacomelli[2], W.R. Gibson[13], D.M. Gingrich[30,a], D. Glenzinski[9], J. Goldberg[22], W. Gorn[4], C. Grandi[2], K. Graham[28], E. Gross[26], J. Grunhaus[23], M. Gruwé[27], C. Hajdu[31] G.G. Hanson[12], M. Hansroul[8], M. Hapke[13], K. Harder[27], A. Harel[22], C.K. Hargrove[7], M. Harin-Dirac[4], M. Hauschild[8], C.M. Hawkes[1], R. Hawkings[27], R.J. Hemingway[6], G. Herten[10], R.D. Heuer[27], M.D. Hildreth[8], J.C. Hill[5], P.R. Hobson[25], A. Hocker[9], K. Hoffman[8], R.J. Homer[1], A.K. Honma[28,a], D. Horváth[31,c], K.R. Hossain[30], R. Howard[29], P. Hüntemeyer[27], P. Igo-Kemenes[11], D.C. Imrie[25], K. Ishii[24], F.R. Jacob[20], A. Jawahery[17], H. Jeremie[18], M. Jimack[1], C.R. Jones[5], P. Jovanovic[1], T.R. Junk[6], N. Kanaya[24], J. Kanzaki[24], D. Karlen[6], V. Kartvelishvili[16], K. Kawagoe[24], T. Kawamoto[24], P.I. Kayal[30], R.K. Keeler[28], R.G. Kellogg[17], B.W. Kennedy[20], D.H. Kim[19], A. Klier[26], T. Kobayashi[24], M. Kobel[3,d], T.P. Kokott[3], M. Kolrep[10], S. Komamiya[24], R.V. Kowalewski[28], T. Kress[4], P. Krieger[6], J. von Krogh[11], T. Kuhl[3], P. Kyberd[13], G.D. Lafferty[16], H. Landsman[22], D. Lanske[14], J. Lauber[15], I. Lawson[28], J.G. Layter[4], D. Lellouch[26], J. Letts[12], L. Levinson[26], R. Liebisch[11], J. Lillich[10], B. List[8], C. Littlewood[5], A.W. Lloyd[1], S.L. Lloyd[13], F.K. Loebinger[16], G.D. Long[28], M.J. Losty[7], J. Lu[29], J. Ludwig[10], D. Liu[12], A. Macchiolo[18], A. Macpherson[30], W. Mader[3], M. Mannelli[8], S. Marcellini[2], T.E. Marchant[16], A.J. Martin[13], J.P. Martin[18], G. Martinez[17], T. Mashimo[24], P. Mättig[26], W.J. McDonald[30], J. McKenna[29], E.A. Mckigney[15], T.J. McMahon[1], R.A. McPherson[28], F. Meijers[8], P. Mendez-Lorenzo[33], F.S. Merritt[9], H. Mes[7], I. Meyer[5], A. Michelini[2], S. Mihara[24], G. Mikenberg[26], D.J. Miller[15], W. Mohr[10], A. Montanari[2], T. Mori[24], K. Nagai[8], I. Nakamura[24], H.A. Neal[12,g], R. Nisius[8], S.W. O'Neale[1], F.G. Oakham[7], F. Odorici[2], H.O. Ogren[12], A. Okpara[11], M.J. Oreglia[9], S. Orito[24], G. Pásztor[31], J.R. Pater[16], G.N. Patrick[20], J. Patt[10], R. Perez-Ochoa[8], S. Petzold[27], P. Pfeifenschneider[14], J.E. Pilcher[9], J. Pinfold[30], D.E. Plane[8], P. Poffenberger[28], B. Poli[2], J. Polok[8], M. Przybycień[8,e], A. Quadt[8], C. Rembser[8], H. Rick[8], S. Robertson[28], S.A. Robins[22], N. Rodning[30], J.M. Roney[28], S. Rosati[3], K. Roscoe[16], A.M. Rossi[2], Y. Rozen[22], K. Runge[10], O. Runolfsson[8], D.R. Rust[12], K. Sachs[10], T. Saeki[24], O. Sahr[33], W.M. Sang[25], E.K.G. Sarkisyan[23], C. Sbarra[29], A.D. Schaile[33], O. Schaile[33], P. Scharff-Hansen[8], J. Schieck[11], S. Schmitt[11], A. Schöning[8], M. Schröder[8], M. Schumacher[3], C. Schwick[8], W.G. Scott[20], R. Seuster[14], T.G. Shears[8], B.C. Shen[4], C.H. Shepherd-Themistocleous[5], P. Sherwood[15], G.P. Siroli[2], A. Skuja[17], A.M. Smith[8], G.A. Snow[17], R. Sobie[28], S. Söldner-Rembold[10,f], S. Spagnolo[20], M. Sproston[20], A. Stahl[3], K. Stephens[16], K. Stoll[10], D. Strom[19], R. Ströhmer[33], B. Surrow[8], S.D. Talbot[1], P. Taras[18],

1

S. Tarem[22], R. Teuscher[9], M. Thiergen[10], J. Thomas[15], M.A. Thomson[8], E. Torrence[8],
S. Towers[6], T. Trefzger[33], I. Trigger[18], Z. Trócsányi[32,h], E. Tsur[23], M.F. Turner-Watson[1],
I. Ueda[24], R. Van Kooten[12], P. Vannerem[10], M. Verzocchi[8], H. Voss[3], F. Wäckerle[10],
A. Wagner[27], D. Waller[6], C.P. Ward[5], D.R. Ward[5], P.M. Watkins[1], A.T. Watson[1],
N.K. Watson[1], P.S. Wells[8], N. Wermes[3], D. Wetterling[11] J.S. White[6], G.W. Wilson[16],
J.A. Wilson[1], T.R. Wyatt[16], S. Yamashita[24], V. Zacek[18], D. Zer-Zion[8]

[1]School of Physics and Astronomy, University of Birmingham, Birmingham B15 2TT, UK
[2]Dipartimento di Fisica dell' Università di Bologna and INFN, I-40126 Bologna, Italy
[3]Physikalisches Institut, Universität Bonn, D-53115 Bonn, Germany
[4]Department of Physics, University of California, Riverside CA 92521, USA
[5]Cavendish Laboratory, Cambridge CB3 0HE, UK
[6]Ottawa-Carleton Institute for Physics, Department of Physics, Carleton University, Ottawa, Ontario K1S 5B6, Canada
[7]Centre for Research in Particle Physics, Carleton University, Ottawa, Ontario K1S 5B6, Canada
[8]CERN, European Organisation for Particle Physics, CH-1211 Geneva 23, Switzerland
[9]Enrico Fermi Institute and Department of Physics, University of Chicago, Chicago IL 60637, USA
[10]Fakultät für Physik, Albert Ludwigs Universität, D-79104 Freiburg, Germany
[11]Physikalisches Institut, Universität Heidelberg, D-69120 Heidelberg, Germany
[12]Indiana University, Department of Physics, Swain Hall West 117, Bloomington IN 47405, USA
[13]Queen Mary and Westfield College, University of London, London E1 4NS, UK
[14]Technische Hochschule Aachen, III Physikalisches Institut, Sommerfeldstrasse 26-28, D-52056 Aachen, Germany
[15]University College London, London WC1E 6BT, UK
[16]Department of Physics, Schuster Laboratory, The University, Manchester M13 9PL, UK
[17]Department of Physics, University of Maryland, College Park, MD 20742, USA
[18]Laboratoire de Physique Nucléaire, Université de Montréal, Montréal, Quebec H3C 3J7, Canada
[19]University of Oregon, Department of Physics, Eugene OR 97403, USA
[20]CLRC Rutherford Appleton Laboratory, Chilton, Didcot, Oxfordshire OX11 0QX, UK
[22]Department of Physics, Technion-Israel Institute of Technology, Haifa 32000, Israel
[23]Department of Physics and Astronomy, Tel Aviv University, Tel Aviv 69978, Israel
[24]International Centre for Elementary Particle Physics and Department of Physics, University of Tokyo, Tokyo 113-0033, and Kobe University, Kobe 657-8501, Japan
[25]Institute of Physical and Environmental Sciences, Brunel University, Uxbridge, Middlesex UB8 3PH, UK
[26]Particle Physics Department, Weizmann Institute of Science, Rehovot 76100, Israel
[27]Universität Hamburg/DESY, II Institut für Experimental Physik, Notkestrasse 85, D-22607 Hamburg, Germany
[28]University of Victoria, Department of Physics, P O Box 3055, Victoria BC V8W 3P6, Canada
[29]University of British Columbia, Department of Physics, Vancouver BC V6T 1Z1, Canada
[30]University of Alberta, Department of Physics, Edmonton AB T6G 2J1, Canada
[31]Research Institute for Particle and Nuclear Physics, H-1525 Budapest, P O Box 49, Hungary

^{32}Institute of Nuclear Research, H-4001 Debrecen, P O Box 51, Hungary
^{33}Ludwigs-Maximilians-Universität München, Sektion Physik, Am Coulombwall 1, D-85748 Garching, Germany

^{a} and at TRIUMF, Vancouver, Canada V6T 2A3
^{b} and Royal Society University Research Fellow
^{c} and Institute of Nuclear Research, Debrecen, Hungary
^{d} on leave of absence from the University of Freiburg
^{e} and University of Mining and Metallurgy, Cracow
^{f} and Heisenberg Fellow
^{g} now at Yale University, Dept of Physics, New Haven, USA
^{h} and Department of Experimental Physics, Lajos Kossuth University, Debrecen, Hungary.

1 Introduction

Measurements of fermion-pair production in e⁺e⁻ collisions at high energies provide an important test of Standard Model predictions, and allow limits to be set on many possible new physics processes [2, 1, 3]. In this paper we present measurements of cross-sections and angular distributions for hadronic and lepton pair final states at a centre-of-mass energy $\sqrt{s}$ near 189 GeV; forward-backward asymmetries for the leptonic states are also given. The data were collected by the OPAL detector at LEP in 1998.

The analyses presented here are essentially the same as those already presented at lower energies [1,2]. We use identical techniques to measure s', the square of the centre-of-mass energy of the e⁺e⁻ system after initial-state radiation, and to separate 'non-radiative' events, which have little initial-state radiation, from 'radiative return' to the Z peak. As at 183 GeV [1], we define non-radiative events as those having $s'/s > 0.7225$, and inclusive measurements are corrected to $s'/s > 0.01$. We correct our measurements of hadronic, $\mu^+\mu^-$ and $\tau^+\tau^-$ events for the effect of interference between initial- and final-state radiation, as in our previous publications, and also use the same treatment of the four-fermion contribution to the two-fermion final states. Because of ambiguities arising from the t-channel contribution, for the e⁺e⁻ final state the acceptance is defined in terms of the angle θ of the electron or positron with respect to the electron beam direction and the acollinearity angle θ_{acol} between the electron and positron. Cross-sections and asymmetries for e⁺e⁻ are not corrected for interference between initial- and final-state radiation; they are compared to theoretical predictions which include interference. With the higher luminosity and hence higher statistics available at 189 GeV we have been able to reduce the experimental systematic errors in some channels, compared with previous analyses.

Measurements of fermion-pair production up to 183 GeV have shown very good agreement with Standard Model expectations [2, 1, 3]. Here we repeat our measurement of the electromagnetic coupling constant $\alpha_{\mathrm{em}}(\sqrt{s})$ including the higher energy data. Including data at 189 GeV also allows us to extend the searches for new physics presented in [1]. In particular we obtain improved limits on the energy scale of a possible four-fermion contact interaction. We also present results of a search for particles which couple to leptons, such as scalar neutrinos (sneutrinos) in theories with R-parity violation. These analyses are updates of those already presented in [1]. Recently it has been pointed out that the quantum-gravity scale could be as low as the electroweak scale with gravitons propagating in extra dimensions [4]. Indirect effects of such gravitational interactions might be seen at colliders [5]. In this paper we present a new search for the possible effects of the gravitational interaction in extra dimensions on the $\mu^+\mu^-$ and $\tau^+\tau^-$ final states. We have obtained lower limits on the effective Planck scale in the space with extra dimensions.

The paper is organized as follows. In Section 2 we describe the data analysis, cross-section and asymmetry measurements. Since the analyses are essentially the same as in [2, 1] we give only a brief description of any changes. In the earlier analyses the errors were generally dominated by statistics, but with the much larger data sample available at 189 GeV the systematic errors are now often comparable with the statistical ones. We therefore discuss the estimation of systematic errors in some detail. In Section 3 we compare our measurements to the predictions of the Standard Model and use them to measure the energy dependence of α_{em}. The results of searches for new physics are presented in Section 4.

2 Data Analysis

The OPAL detector[1], trigger and data acquisition system are fully described elsewhere [6–10]. The high redundancy of the trigger system leads to negligible trigger inefficiency for all channels discussed here. The analyses presented in this paper use more than 180 pb^{-1} of data collected at centre-of-mass energies near 189 GeV during 1998; the actual amount of data varies from channel to channel. The luminosity-weighted mean centre-of-mass energy is 188.63±0.04 GeV [11].

Selection efficiencies and backgrounds were calculated using Monte Carlo simulations. The default set of generators used is identical to that in [1]. Use of alternative generators in assessing sytematic errors is discussed below. All events were passed through a full simulation [12] of the OPAL detector and processed as for real data.

The luminosity was measured using small-angle Bhabha scattering events recorded in the silicon-tungsten luminometer [8,2]. The overall error on the luminosity measurement amounts to 0.21%, arising from data statistics (0.09%), knowledge of the theoretical cross-section (0.12%), experimental systematics (0.15%) and uncertainty in the beam energy (0.04%). The theoretical cross-section is calculated using BHLUMI 4.04 [13], and a recent assessment of the theoretical error associated with this program [14] has resulted in a significant decrease in this contribution compared with earlier analyses. Errors from the luminosity measurement are included in all the systematic errors on cross-sections quoted in this paper, and correlations between measurements arising from the luminosity determination are included in all fits.

2.1 Cross-section and Asymmetry Measurements

Hadronic, e^+e^-, $\mu^+\mu^-$ and $\tau^+\tau^-$ events were selected using the same criteria[2] as at 183 GeV [1]. Distributions of $\sqrt{s'}$ for each channel, determined using kinematic fits for hadrons and track angles for the lepton pairs as in [2], are shown in Fig. 1. Efficiencies, backgrounds and feedthrough of events from lower s' into the non-radiative samples were calculated from Monte Carlo simulation, and are given in Table 1. Efficiencies determined from two-fermion Monte Carlo events have been corrected for the effect of the four-fermion contribution as described in [2]. In addition, a small correction ($\sim$0.4%) has been applied to the relevant electron pair efficiencies to account for tracking problems in regions of the detector near anode planes of the central jet chamber. The numbers of selected events and the measured cross-sections are presented in Table 2. The evaluation of the systematic errors is described in detail below. As well as cross-sections for $q\overline{q}$ events, we also present a fully inclusive hadronic cross-section $\sigma(q\overline{q}X)$. This uses the same event selection as is used for $q\overline{q}$ events but W-pairs are not rejected. The cross-section therefore includes W-pair (and Z-pair) production with at least one W (Z) decaying hadronically, but does not include other four-fermion hadronic events (for example from two-photon processes) which are treated as background. The energy dependence of the measured cross-section for each channel is shown in Figs. 2–5.

---

[1]OPAL uses a right-handed coordinate system in which the z axis is along the electron beam direction and the x axis is horizontal. The polar angle θ is measured with respect to the z axis and the azimuthal angle ϕ with respect to the x axis.

[2]In the selection of muon pairs a minor change was made to the cut used to reject cosmic ray events having back-to-back hits in the time-of-flight counters. This change reduced the cosmic ray background in the selected events, allowing a reduction in the associated systematic error of around 40%.

Measurements of the forward-backward asymmetry for lepton pairs are given in Table 3 and compared with lower energy measurements in Fig. 6. The values for muon and tau pairs are obtained by averaging the results measured using the negative particle with those obtained using the positive particle to reduce systematic effects. Muon and tau asymmetries are corrected to the full angular range by applying a multiplicative correction obtained from ZFITTER to the asymmetry measured within the acceptance of the selection cuts ($|\cos\theta| < 0.95$ for muon pairs, $|\cos\theta| < 0.9$ for tau pairs). The angular distribution of the primary quark in non-radiative hadronic events is given in Table 4, and the corrected angular distributions for the lepton pairs are given in Tables 5 and 6. The angular distributions are plotted in Fig. 7.

All cross-sections and asymmetries except those for e^+e^- have been corrected for the contribution of interference between initial- and final-state radiation as described in [2][3]. The corrections are shown in Table 7.

2.2 Systematic Studies

2.2.1 Hadronic Events

The selection criteria for hadronic events [1,2] use the multiplicity of tracks and electromagnetic calorimeter clusters, the total electromagnetic calorimeter energy and the energy balance along the beam direction. Events selected as W-pair candidates according to the criteria of [20] are rejected. In selecting the non-radiative sample a kinematic fit is used to determine s'. The main backgrounds arise from four-fermion final states.

The systematic errors on the hadronic cross-sections have been substantially reassessed compared with lower energy analyses. They are summarized in Table 8, and the main contributions are discussed below.

ISR modelling. The effect of the modelling of initial-state radiation on the selection efficiency and s' determination has been estimated by comparing the prediction of PYTHIA [21] with that of the KK2f [22] Monte Carlo generator, which has a more complete description of initial-state radiation. The difference between the two was taken as the systematic error.

Fragmentation modelling. The effect of the hadronization model on the efficiency of the non-radiative selection has been investigated by comparing the string fragmentation implemented in PYTHIA with the cluster model of HERWIG [23]. In order to decouple the effects of hadronization from differences in initial-state radiation treatment in the two programs, efficiencies were compared in bins of s'. They were found to agree within the statistical precision of the test, which was accordingly assigned as the error. In the inclusive selection, the greatest loss of efficiency comes from the cut on electromagnetic calorimeter energy. A comparison of jets in Z data and Monte Carlo showed that this is well simulated by JETSET (but not by HERWIG). Therefore the systematic error was estimated by changing the energy scale in the Monte Carlo by the observed difference between data and JETSET and re-evaluating the efficiency. In addition, the effect of a conservative variation of one unit in charged particle multiplicity was also taken into account in the inclusive case.

---

[3]The corrections in our earlier publications [2, 1] were based on the interference cross-sections predicted by ZFITTER version 5.0, which have subsequently been found by the authors to be a factor of three too big for hadronic final states. We have therefore reduced the interference corrections applied to the 130–183 GeV hadronic cross-sections by a factor of three when using these data in the fits described in this paper.

Detector effects. The selection of inclusive events is mainly based on the electromagnetic calorimeter, and is thus sensitive to the energy scale of the calorimeter, and any angular dependence of the energy scale. The energy scale in hadronic events has been studied using data taken at the Z peak in 1998. The energy scales in data and Monte Carlo agree to better than 0.5%, and the systematic error on the efficiency for inclusive events was estimated by changing the energy scale in data by this amount. For non-radiative events, a kinematic fit is used to determine s', which thus depends on jet energies, angles and their errors. Studies of data taken at the Z peak were again used to assess the uncertainties in these; in addition, studies of Bhabha events were used to determine similar uncertainties in the photon energies and angles and their resolution. The systematic error in the non-radiative events was determined by changing each of these quantities and re-evaluating s'.

s' determination. Any possible systematic effects in the determination of s' not covered by the above ISR, fragmentation and detector systematics were assessed by changing the method of calculating s'. The algorithm was changed to allow for only a single radiated photon, the cuts used to identify isolated photons in the detector were varied, the value of the resolution parameter used in the jet finding was varied, and for jets in the forward regions whose energies are poorly measured the kinematic fit was compared with the calculation of s' using jet angles. In each case, the modified algorithm was applied to data and Monte Carlo, and the cross-section recomputed. The changes observed were in all cases compatible with statistical fluctuations. The largest of these, averaging over data taken at 189 GeV and at lower energies, was taken as a systematic error.

WW rejection cuts and WW background. The systematic error arising from the effect of the W-pair rejection cuts on the efficiency, and the uncertainty in the remaining W-pair background, were estimated in a similar manner to that described in [20]. As a cross-check, we have calculated the hadronic cross-sections without rejecting W-pair events, by subtracting their expected contribution instead. The measured values of 99.6±0.9±1.2 pb ($s'/s > 0.01$) and 22.44±0.42±0.20 pb ($s'/s > 0.7225$), after correction for interference between initial- and final-state radiation, are in good agreement with the values in Table 2.

Background. Uncertainties in other background contributions were estimated by comparing the predictions of various generators. In the inclusive sample the largest uncertainty arises from the contribution of two-photon events. At low Q^2 the generators PYTHIA and PHOJET [24] were compared. At high Q^2 the TWOGEN [25] program (with the 'perimiss' option [26]), PYTHIA, HERWIG and PHOJET were used. In the non-radiative sample the main background arises from four-fermion final states. The prediction of grc4f [27] was compared with that of EXCALIBUR [28].

Interference. The uncertainty arising from the removal of the contribution from interference between initial- and final-state radiation was estimated as described in [2].

2.2.2 Electron Pairs

Electron pair events are required to have low multiplicity and large energy deposited in the electromagnetic calorimeter. The 'large acceptance' selection ($|\cos\theta| < 0.96$, $\theta_{\mathrm{acol}} < 10°$) does not require tracks associated to electromagnetic calorimeter clusters, but all other selections require two of the three highest energy clusters to have an associated track. For measurements of the asymmetry and angular distribution these tracks are required to have opposite charge.

The systematic errors associated with the electron pair measurements are summarized in Table 9. The most important ones are discussed below.

Four-fermion contribution. The full size of the difference in efficiency from including s-channel four-fermion events in the signal definition was included as a systematic error.

Multiplicity cuts. The errors arising from the requirement of low multiplicity have been estimated by varying the multiplicity cuts used by ± 1 unit.

Calorimeter energy scale and resolution. A detailed comparison between data and Monte Carlo has been made of the energy scale and resolution of the electromagnetic calorimeter, and the results of this study used to assess possible effects on the selection efficiency. Typically the energy scale was varied by 0.3% and the resolution by 10% of its value.

Track requirements. Matching between tracks and clusters has been studied using events passing all selection cuts, except that only one of the three highest energy clusters has an associated track. These are expected to be mainly $e^+e^-\gamma$ final states where one electron and the photon lie within the acceptance and $\gamma\gamma$ final states where one photon has converted in the detector, with small contributions from other final states. An excess of such events was seen in data compared with Monte Carlo expectation; this excess amounted to approximately 0.8% of the number of events passing all cuts. Roughly half the excess is concentrated in regions of ϕ near the anode planes of the central jet chamber, and arises from track reconstruction problems in this region. The other half could arise from track reconstruction problems, or could arise from problems modelling $e^+e^-\gamma$ or $\gamma\gamma$ events. For each acceptance region we take half the difference between data and Monte Carlo as a correction to the efficiency to account for the loss of tracks near jet chamber anode planes, and assign the other half as a systematic error associated with track requirements.

Acceptance correction. Because of the steepness of the angular distribution, uncertainties in the determination of θ are an important systematic error. These have been assessed by comparing measurements of θ in the electromagnetic calorimeter with those in the central tracking chambers and the muon chambers. These studies indicate a possible bias in the θ reconstruction of electromagnetic clusters of around 1 mrad in the endcap region of the detector. The effect of the observed biases on the acceptance was calculated using Monte Carlo events, and assigned as a systematic error associated with the acceptance correction.

Background The dominant background in the selections including tracks is from $\tau^+\tau^-$ events if a tight acollinearity cut is applied. With a loose acollinearity cut, $e^+e^-\gamma$ and $e^+e^-e^+e^-$ events are also significant. The systematic error arising from uncertainty in the background has been assessed by comparing the numbers of events in data and Monte Carlo which pass all cuts except the cut on total calorimeter energy; these events are predominantly background. In each acceptance region, the numbers agree to within one standard deviation, and the statistical precision of the test was taken as the associated systematic error. For the selection which does not use tracks, the only important background is from $\gamma\gamma$ final states; here we used the statistical precision of the OPAL cross-section measurement [29] to estimate the systematic error from this background.

The systematic error on the overall normalization of the angular distribution has been assessed in a similar manner to those on the cross-sections, but includes an extra contribution from an observed difference of 0.5% between data and Monte Carlo in the probability of the two tracks having opposite charge. The overall error amounts to 0.76%.

Systematic errors on the asymmetry measurement arise from the effects of θ mismeasurement, charge misassigment and background and efficiency corrections, and amount to 0.005. Even with the current statistics this is only half of the statistical error.

2.2.3 Muon and Tau Pairs

Muon pair events are required to have two tracks identified as muons. Background from cosmic ray events is removed using time-of-flight counters and vertex cuts, and two-photon events are rejected by placing a cut on the total visible energy.

The selection of tau pair events uses information from the central tracking detectors and electromagnetic calorimeter to identify events with two collimated, low multiplicity jets. Background from Bhabha events is rejected using cuts on the total visible energy and the electromagnetic calorimeter energy associated with each tau cone. Two-photon events are rejected using cuts on total visible energy and missing momentum.

Systematic errors on the muon pair and tau pair cross-sections are summarized in Tables 10 and 11 respectively. They were estimated using similar methods, and the main contributions are discussed below.

Efficiency. The systematic errors on the efficiencies were evaluated using high statistics LEP1 data and Monte Carlo samples. The muon pair or tau pair selection cuts were applied to these samples and the difference between the number of data events selected and the number expected from Monte Carlo was used to estimate the systematic error associated with the efficiency. For this comparison, it was necessary to relax some of the cuts which scale with centre-of-mass energy slightly, so that the efficiency for events on the Z peak remained high.

Cosmic background. The error due to any remaining cosmic background in the muon pairs was estimated by varying the time-of-flight or vertex cuts by amounts determined from the resolution in the respective variables.

Other backgrounds. The main backgrounds in the muon pairs arise from $e^+e^-\mu^+\mu^-$, $\tau^+\tau^-$ and leptonic four-fermion final states. The largest background in the tau pairs arises from Bhabha events. Other important backgrounds arise from $e^+e^-e^+e^-$ and $e^+e^-\tau^+\tau^-$ final states. Backgrounds were studied by considering distributions of selection variables after all cuts except the one on that variable. The numbers of events in data and Monte Carlo were compared for a region enriched in a particular background, and the difference, or its statistical error, used to estimate the systematic error from that background source. For example, the $e^+e^-\mu^+\mu^-$ background in the muon pairs was studied using the distribution of visible energy; the Bhabha background in the tau pairs was estimated using distributions of total visible energy with the cuts on energy relaxed. For backgrounds which cannot be studied in this way, we conservatively assume an error of 50%.

Interference. The uncertainty arising from the removal of the contribution from interference between initial- and final-state radiation was estimated as described in [2].

3   Comparison with Standard Model Predictions

The cross-section and asymmetry measurements at 189 GeV are compared with the Standard Model predictions in Tables 2 and 3 respectively. Figures 2–5 show cross-sections, for both

inclusive and non-radiative events, as a function of $\sqrt{s}$, while Fig. 6 shows the measured asymmetry values. The Standard Model predictions are calculated using ALIBABA [16] for the e^+e^- final state and ZFITTER [15] for all other final states; in this paper we use ZFITTER version 6.10 with input parameters as in [2], except that the mass of the Higgs boson is set to 175 GeV, roughly midway between the experimental lower bound [30] and the 95% confidence level upper limit from electroweak fits [31]. Values predicted by the TOPAZ0 [32] program are higher than those predicted by ZFITTER by about 0.03% (0.2%) for non-radiative (inclusive) muon and tau pair cross-sections, and by about 0.6% (0.8%) for the non-radiative (inclusive) hadronic cross-section. A major theoretical uncertainty on these cross-sections arises from the contribution of virtual pairs. By comparing the predictions of ZFITTER for the sum of real and virtual pairs with that of the four-fermion Monte Carlo grc4f for real pairs, we estimate this contribution to be around –0.6% of the muon or tau pair cross-section, independent of the s' cut. In the fits described below we therefore assign the full size of this contribution, 0.6%, as the theoretical error on non-radiative muon and tau pair cross-sections. For non-radiative hadrons, we combine the size of the virtual pair contribution with the difference seen between the ZFITTER and TOPAZ0 programs to give a theoretical error of 0.8%. In the case of electron pairs, we have compared the predictions of ALIBABA with those of TOPAZ0, and also with those of the BHWIDE [33] Monte Carlo program. Based on these comparisons, we assign a theoretical error of 2% to electron pairs in the fits below. For the muon and tau pair asymmetries, we use a theoretical error of 0.005, based on comparisons between ZFITTER, TOPAZ0 and the KK2f Monte Carlo program. The agreement between the measured cross-sections and Standard Model predictions is generally good.

The angular distributions for all channels at 189 GeV are compared with Standard Model predictions in Fig. 7. In the case of electron pairs, we also show the distribution which would be expected if there were no contribution from the t-channel Z-exchange diagram. We clearly see that the contribution of this diagram is necessary to reproduce the measured distribution.

In Fig. 8 we show the ratio of measured hadronic cross-sections to theoretical muon pair cross-sections as a function of centre-of-mass energy for two cases. In the first case the numerator of this ratio is the inclusive q$\overline{q}$X cross-section, in the second case it is the non-radiative q$\overline{q}$ cross-section corrected to the Born level[4]. In each case the denominator is the corresponding muon pair cross-section calculated using ZFITTER. The inclusive ratio clearly shows the effect of W^+W^- production.

3.1 Energy Dependence of α_{em}

Non-radiative cross-section and asymmetry measurements have been used to measure the electromagnetic coupling constant α_{em} at LEP2 energies, as described in [2, 1]. We form the χ^2 between measured values and the Standard Model predictions calculated as a function of $\alpha_{\mathrm{em}}(\sqrt{s})$ using ZFITTER, with all other ZFITTER input parameters fixed. Correlations between measurements are fully taken into account. We perform two fits. The first one uses only the measurements of hadronic, $\mu^+\mu^-$ and $\tau^+\tau^-$ cross-sections and the combined muon and tau asymmetry values, for $s'/s > 0.7225$, presented here. The second fit also includes data at 130–183 GeV [1, 2]; in this combined fit α_{em} runs with energy with a slope corresponding to the fitted value. The results of both fits are given in Table 12, and measured values of α_{em}

---

[4]Born level means the cross-section obtained from the improved Born approximation before convolution with QED radiation; electroweak and QCD corrections are included.

are shown in Fig. 9. They are consistent with the Standard Model expectation. The value of $1/\alpha_{\rm em}$ obtained from the combined measurements is 3.4 standard deviations below the low energy limit of 137.0359979±0.0000032 [39].

The combined fit described above uses measurements of cross-sections which depend on the measurement of luminosity, which itself assumes the Standard Model running of $\alpha_{\rm em}$ from $(Q^2 = 0)$ to typically $Q^2 = (3.5\ {\rm GeV})^2$, where $1/\alpha_{\rm em} \simeq 134$. Therefore it measures the running of $\alpha_{\rm em}$ only from $Q_{\rm lumi} \simeq 3.5$ GeV onwards. As before, to become independent of the luminosity measurement, we have repeated the combined fit replacing the cross-sections for hadrons, muon and tau pairs with the ratios $\sigma(\mu\mu)/\sigma(q\overline{q})$ and $\sigma(\tau\tau)/\sigma(q\overline{q})$. This is possible since, above the Z peak, hadrons and leptons have very different sensitivity to $\alpha_{\rm em}$ as discussed in [2]. The result of this fit is $1/\alpha_{\rm em}(181.94\ {\rm GeV}) = 126.2^{+3.5}_{-3.2}$, with a χ^2 of 11.8 for 18 degrees of freedom. The value is close to that obtained from the cross-section fit but with somewhat larger errors. The difference in χ^2 between the best fit and the assumption that $\alpha_{\rm em}$ does not run with energy but is fixed at the low energy limit is 7.88. If $\alpha_{\rm em}$ did not run with energy, the probability of measuring $1/\alpha_{\rm em} = 126.2$ or lower would be 0.25%, thus demonstrating the running of $\alpha_{\rm em}$ from $(Q^2 = 0)$ to LEP2 energies. This measurement of $\alpha_{\rm em}$ is independent of low-mass hadronic loops and nearly independent of the mass of the Higgs boson and $\alpha_{\rm s}$; it can be scaled to the mass of the Z, giving $1/\alpha_{\rm em}(91.19\ {\rm GeV}) = 127.4^{+3.2}_{-2.9}$.

4 Constraints on New Physics

Deviations of the measured data from Standard Model predictions would be an indication of new physics processes. The good agreement between data and the Standard Model places severe constraints on the energy scale of new phenomena. In this section we report the results of three analyses in which limits are set on various new physics processes. Firstly we consider a four-fermion contact interaction. This offers an appropriate framework for searching for the effects of the exchange of a new particle with mass $m_{\rm X} \gg \sqrt{s}$. Limits on the energy scale Λ are presented for various models. For lower mass ranges, $\sqrt{s} \lesssim m_{\rm X} < \Lambda$, propagator and width effects must be taken into account. The results of a search for heavy particles which couple to leptons are reported. Finally we present the results of a search for the indirect effects of the gravitational interaction in extra dimensions on the $\mu^+\mu^-$ and $\tau^+\tau^-$ final states.

4.1 Limits on Four-fermion Contact Interactions

A very general framework in which to search for the effect of new physics is the four-fermion contact interaction. In this framework [40] the Standard Model Lagrangian for $e^+e^- \rightarrow f\overline{f}$ is extended by a term describing a new effective interaction with an unknown coupling constant g and an energy scale Λ:

$$\mathcal{L}^{\rm contact} = \frac{g^2}{(1+\delta)\Lambda^2} \sum_{i,j={\rm L,R}} \eta_{ij}[\overline{e}_i\gamma^\mu e_i][\overline{f}_j\gamma_\mu f_j], \qquad (1)$$

where $\delta = 1$ for $e^+e^- \rightarrow e^+e^-$ and $\delta = 0$ otherwise. Here $e_{\rm L}(f_{\rm L})$ and $e_{\rm R}(f_{\rm R})$ are chirality projections of electron (fermion) spinors, and η_{ij} describes the chiral structure of the interaction. The parameters η_{ij} are free in these models, but typical values are between -1 and $+1$, depending on the type of theory assumed [41]. Here we consider the same set of models as in [2].

We have repeated the analysis described in [2], including the measurements of the angular distributions for the non-radiative $e^+e^- \rightarrow e^+e^-$, $e^+e^- \rightarrow \mu^+\mu^-$, $e^+e^- \rightarrow \tau^+\tau^-$ processes and the non-radiative cross-section for $e^+e^- \rightarrow q\overline{q}$ at 189 GeV presented here. As before, we used a maximum likelihood fit in the case of the lepton angular distributions, and a χ^2 fit for the hadronic cross-sections. Radiative corrections to the lowest order cross-section were taken into account as described in [2]. Theoretical uncertainties in the Standard Model predictions were taken into account as discussed in Section 3. Limits on the energy scale Λ were extracted assuming $g^2/4\pi = 1$.

The results are shown in Table 13 and illustrated graphically in Fig. 10; the notation for the different models is identical to [42,2]. The two sets of values Λ_+ and Λ_- shown in Table 13 correspond to positive and negative values of $\varepsilon = 1/\Lambda^2$ respectively, reflecting the two possible signs of η_{ij} in Equation (1). As before, the data are particularly sensitive to the VV and AA models; the combined data give limits on Λ in the range 10–14 TeV for these models. For the other models the limits generally lie in the range 7–10 TeV. These limits are roughly 1–2 TeV above those from the 130–183 GeV data alone.

Contact interactions involving quarks have also been studied in ep and pp collisions, where limits comparable to our values are found [45,44]. Atomic physics parity violation experiments can place higher limits ($\simeq$ 15 TeV [46]) on models of eeuu and eedd contact interactions which violate parity.

4.2 Limits on Heavy Particles Coupling to Leptons

In this section we present the results of a search under the explicit assumption that any new phenomena are due to a heavy particle which couples to leptons. Although we use specific particles in the analysis presented below, the results are generally applicable for any heavy particle with similar properties.

Examples of particles which couple to leptons are sneutrinos with R-parity violating couplings. These couplings are given by the term $\lambda_{ijk} L_L^i L_L^j \overline{E}_R^k$ of the superpotential [47], where the indices i, j, k denote the family of the particles involved, L_L^i and L_L^j are the SU(2) doublet lepton superfields and $\overline{E}_R^k$ denotes an antilepton singlet superfield. The couplings λ_{ijk} are non-vanishing only for $i < j$, so at least two different generations of leptons are coupled in purely leptonic vertices.

Sneutrinos may contribute to leptonic cross-sections via both s-channel and t-channel diagrams, depending on the type of sneutrino and the final state considered. Processes involving an s-channel diagram lead to resonant behaviour when the centre-of-mass energy is near the sneutrino mass, and hence more stringent limits can be set than for processes involving only t-channel diagrams. Here we consider two typical cases involving an s-channel diagram:

- the presence of a $\tilde{\nu}_\tau$ which interacts via the coupling λ_{131} giving rise to a change in the e^+e^- cross-section via an s-channel and a t-channel process; the limits obtained for this case could equally apply to a $\tilde{\nu}_\mu$ interacting via the coupling λ_{121};

- a $\tilde{\nu}_\tau$ with the couplings λ_{131} and λ_{232} both different from zero. In the analysis both couplings are assumed to be of equal size[5]. Such a scenario gives rise to a modified $\mu^+\mu^-$

---

[5]Both couplings violate conservation of the same lepton flavours so that this scenario is compatible with the experimental observation of lepton number conservation.

cross-section due to an *s*-channel exchange of the sneutrino.

To calculate the differential cross-sections for these processes we use the formulae in [48], taking radiative corrections into account as in the contact interaction analysis.

In each case we use a maximum likelihood fit of the model prediction to data and extract 95% confidence level limits on the coupling as a function of the sneutrino mass. We include in the fits the data at 189 GeV presented here and the data at 130–183 GeV presented in [2,1]. We use the full $\sqrt{s'}$ distributions as described in [1] in order to improve the sensitivity at values of sneutrino mass between the centre-of-mass energies of LEP. The inclusion of asymmetry values has a very small effect on the limits, therefore we present only limits excluding asymmetry measurements in order not to lose generality.

The limits on λ_{131} derived from the e$^+$e$^-$ data are shown in Fig. 11. They are in the range 0.01 – 0.12 for $100 < m_{\tilde{\nu}} < 200$ GeV. For masses above 200 GeV there is no *s*-channel contribution, and the limits rise to 0.16 at 300 GeV. Figure 12 shows limits on $\lambda_{131} = \lambda_{232}$ derived from the $\mu^+\mu^-$ data. These are in the range 0.02 – 0.08 for $100 < m_{\tilde{\nu}} < 200$ GeV, rising to 0.28 at 300 GeV. The fine structure in the region $m_{\tilde{\nu}} < 200$ GeV results from fluctuations in the s' distributions. These limits are valid for sneutrino widths of 1 GeV or less. The inclusion of the 189 GeV data has significantly improved the limits for masses near 189 GeV.

Direct searches [49] for sneutrinos with *R*-parity violating couplings can exclude a $\tilde{\nu}_e$ with mass less than 80 GeV and a $\tilde{\nu}_\mu$ with mass less than 58 GeV. Our results place limits on the couplings for masses above 100 GeV.

4.3   Gravitational Interaction in Extra Dimensions

In nature there are two fundamental scales which differ by many orders of magnitude, the ratio between the Planck scale ($M_{\rm Pl} \sim 10^{18-19}$ GeV) and the electroweak scale ($M_{\rm EW} \sim 10^{2-3}$ GeV) being about 10^{16}. The lack of explanation of this fact is known as the 'hierarchy problem'. Recently it has been pointed out that the quantum-gravity scale could be as low as the electroweak scale with gravitons propagating in a compactified higher dimensional space [4], while other Standard Model particles are confined to the usual $3 + 1$ space-time dimensions. According to this theory the Planck mass in $D = n + 4$ dimensions ($M_{\rm D}$) is chosen to be the electroweak scale, so that the hierarchy problem is solved by definition. The Planck mass in the usual 4 space-time dimensions is given by

$$M_{\rm Pl}^2 = R^n M_{\rm D}^{n+2}. \tag{2}$$

where R is the compactification radius of the extra dimensions.

Gravitons may contribute to two-fermion production via the process e$^+$e$^- \rightarrow$ G$^* \rightarrow$ f$\bar{\rm f}$. Although the contribution from a single graviton state is very small compared with the Standard Model contribution, the very large number of possible excitation modes in the extra dimensions might lead to a measurable effect [5].

The phenomenology of virtual graviton exchange processes in the context of collider experiments is described in [5, 50–52]. The differential cross-section for the production of fermion pairs with the inclusion of virtual graviton exchange can be written generally as

$$\frac{{\rm d}\sigma}{{\rm dcos}\,\theta} = A(\cos\theta) + B(\cos\theta)\left[\frac{\lambda}{M_{\rm s}^4}\right] + C(\cos\theta)\left[\frac{\lambda}{M_{\rm s}^4}\right]^2, \tag{3}$$

where θ is the production polar angle of the fermion with respect to the e^- beam direction and M_s is a mass scale parameter of the order of M_D. This parametrisation is taken from [50] and we consistently use it in this paper. The exact definition of the scale parameter can be found in [5][6]. The parameter λ is of $\mathcal{O}(1)$ and cannot be explicitly calculated without knowledge of the full quantum gravity theory [50]. In contrast to graviton production, $e^+e^- \to G\gamma$, the dependence of the fermion-pair cross-section on the number of extra dimensions is weak and is included in λ. Here we consider the cases $\lambda = +1$ and $\lambda = -1$.

Although the functional form of the new interaction is similar to that of the contact interaction [40], the differential cross-section for the new interaction includes terms proportional to $\cos^3\theta$ or $\cos^4\theta$. The mass scale dependence of the amplitude of the new interaction is $1/(\text{mass scale})^4$, whereas that of the ordinary contact interaction is $1/(\text{mass scale})^2$.

The first term in Equation (3) is the Standard Model prediction, the second term is the interference term and the third is the new interaction term. The coefficients in the above expression are given in [50].

We have analysed the angular distributions of non-radiative muon and tau pair events at 189 GeV, together with the distributions at 183 GeV presented in [1]. To obtain a lower limit on M_s, we performed a binned maximum likelihood fit to angular distributions at the two centre-of-mass energies simultaneously, in a similar manner to the contact interaction analysis in Section 4.1. In order to fit the differential cross-section Equation (3) to the data, a first-order photon radiation correction [53] was applied to the terms B and C. ZFITTER was used to calculate the Standard Model term A. The theoretical cross-section as a function of $\varepsilon \equiv \lambda/M_s^4$ was then converted to the expected number of events in each of the $\cos\theta$ bins, taking into account the event selection efficiency, background, feedthrough of low s' events and the effect of interference between initial- and final-state photon radiation. The likelihood was calculated from the Poisson probability for the observed number of events. Additional Gaussian smearing was taken into account in the likelihood in order to allow the overall normalization error to vary within the systematic errors discussed in Section 2. We assigned a theoretical error of 0.6% to the Standard Model prediction of ZFITTER, as discussed in Section 3.

We derived the 95% confidence level lower limits on M_s from the values of ε corresponding to an increase in the negative log likelihood of 1.92 with respect to the minimum found in the ε region considered. As M_s^4 must be positive, the physically allowed region is $\varepsilon > 0$ for $\lambda = +1$ and $\varepsilon < 0$ for $\lambda = -1$.

The 95% confidence level lower limits on M_s derived from the muon pairs, from the tau pairs, and from a simultaneous fit to the muon and tau pairs, are given in Table 14. They are in the range 0.50–0.68 TeV. The results of the fit to the muon pairs are displayed in Fig. 13, those of the fit to the tau pairs in Fig. 14. In each case we show the measured angular distributions and the ratio of the measurements to the Standard Model predictions, together with curves representing the Standard Model prediction, the best fit, and the distributions corresponding to the 95% confidence level limits on M_s.

Limits on the gravitational interaction in extra dimensions have also been derived from OPAL measurements of photonic final states [29].

---

[6]Note that in the reference by Giudice *et al.* [5] a different notation is used. The scale factor Λ_T in the paper by Giudice *et al.* is defined to be $\Lambda_T^4 = \frac{\pi}{2}\frac{M_s^4}{|\lambda|}$. If the ultra-violet cut-off for graviton exchange is taken as M_D, M_s is essentially the same as M_D except for an $\mathcal{O}(1)$ factor.

5　Conclusions

We have presented new measurements of cross-sections and asymmetries for hadron and lepton pair production in e^+e^- collisions at a centre-of-mass energy of 189 GeV. The results, for both inclusive fermion-pair production and for non-radiative events, are in good agreement with Standard Model expectations. From these and earlier measurements we derive a value for the electromagnetic coupling constant $1/\alpha_{\rm em}(181.94~{\rm GeV}) = 126.8^{+3.0}_{-2.7}$.

The measurements have been used to improve existing limits on new physics. In the context of a four-fermion contact interaction we have improved the limits on the energy scale Λ from typically 2–10 TeV to 3–13 TeV, assuming $g^2/4\pi = 1$. We have also presented limits on new particles such as sneutrinos in supersymmetric theories with R-parity violation which couple to leptons. Sensitivity to sneutrino masses between the centre-of-mass energy points of LEP has been improved by using a complete scan of the s' distribution for processes involving an s-channel diagram. In these cases, limits on the couplings in the range $0.01 - 0.1$ are obtained for $100 < m < 200$ GeV.

In a search for the possible effects of gravitons propagating in extra dimensions, we have obtained lower limits on the effective Planck scale in the space with extra dimensions in the range 0.50–0.68 TeV.

Acknowledgements

References

[1] OPAL Collab., G. Abbiendi et al., Eur. Phys. J. **C6** (1999) 1.

[2] OPAL Collab., K. Ackerstaff et al., Eur. Phys. J. **C2** (1998) 441.

[3] ALEPH Collab., D. Buskulic et al., Phys. Lett. **B378** (1996) 373;
ALEPH Collab., R. Barate et al., *Study of Fermion Pair Production in* e$^+$e$^-$ *Collisions at 130–183 GeV*, CERN-EP/99-042, March 1999, submitted to Eur. Phys. J. C;
DELPHI Collab., P. Abreu et al., *Measurement and Interpretation of Fermion-Pair Production at LEP Energies from 130 to 172 GeV*, CERN-EP/99-05, January 1999, to be published in Eur. Phys. J. C;
L3 Collab., M. Acciarri et al., Phys. Lett. **B370** (1996) 195;
L3 Collab., M. Acciarri et al., Phys. Lett. **B407** (1997) 361;
L3 Collab., M. Acciarri et al., Phys. Lett. **B414** (1997) 373;
L3 Collab., M. Acciarri et al., Phys. Lett. **B433** (1998) 163.

[4] N. Arkani-Hamed, S. Dimopoulos and G. Dvali, Phys. Lett. **B429** (1998) 263;
I. Antoniadis, N. Arkani-Hamed, S. Dimopoulos and G. Dvali, Phys. Lett. **B436** (1998) 257;
N. Arkani-Hamed, S. Dimopoulos and G. Dvali, Phys. Rev. **D59** (1999) 86004.

[5] G.F. Giudice, R. Rattazzi and J.D. Wells, Nucl. Phys. **B544** (1999) 3.

[6] OPAL Collab., K. Ahmet et al., Nucl. Instr. and Meth. **A305** (1991) 275.

[7] S. Anderson et al., Nucl. Instr. and Meth. **A403** (1998) 326.

[8] B.E. Anderson et al., IEEE Trans. Nucl. Sci. **41** (1994) 845.

[9] M. Arignon et al., Nucl. Instr. and Meth. **313** (1992) 103;
M. Arignon et al., Nucl. Instr. and Meth. **333** (1993) 330.

[10] J.T. Baines et al., Nucl. Instr. and Meth. **A325** (1993) 271;
D.G. Charlton, F. Meijers, T.J. Smith, P.S. Wells, Nucl. Instr. and Meth. **A325** (1993) 129.

[11] The LEP Energy Working Group, *Evaluation of the LEP centre-of-mass energy for data taken in 1998*, LEP Energy Working Group 99/01, March 1999;
LEP Energy Working Group, A Blondel et al., CERN-EP/98-191, CERN-SL/98-073, submitted to Eur. Phys. J. C.

[12] J. Allison et al., Nucl. Instr. and Meth. **A317** (1992) 47.

[13] S. Jadach et al., Comp. Phys. Comm. **102** (1997) 229.

[14] W. Placzek, S. Jadach, M. Melles, B.F.L. Ward and S.A.Jost, CERN-TH/99-07.

[15] D. Bardin et al., DESY 99-070;
D. Bardin et al., CERN-TH 6443/92;
D. Bardin et al., Phys. Lett. **B255** (1991) 290;
D. Bardin et al., Nucl. Phys. **B351** (1991) 1;

D. Bardin et al., Z. Phys. **C44** (1989) 493.
We use ZFITTER version 6.10 with default parameters, except `INTF=0`, `FINR=0` and
`ISPP=−1`, and with the following input parameters: m_Z=91.1863 GeV, m_{top}=175 GeV,
m_{Higgs}=175 GeV, $\alpha_s(m_Z)$=0.118.

[16] W. Beenakker et al., Nucl. Phys. **B349** (1991) 323.

[17] OPAL Collab., P.D. Acton et al., Z. Phys. **C58** (1993) 219.

[18] OPAL Collab., R. Akers et al., Z. Phys. **C61** (1994) 19.

[19] OPAL Collab., G. Alexander et al., Z. Phys. **C52** (1991) 175.

[20] OPAL Collab., G. Abbiendi et al., Eur. Phys. J. **C8** (1999) 191.

[21] T. Sjöstrand, Comp. Phys. Comm. **82** (1994) 74.

[22] S. Jadach, B.F.L. Ward and Z. Wąs, Phys. Lett. **B449** (1999) 97.

[23] G. Marchesini et al., Comp. Phys. Comm. **67** (1992) 465.

[24] R. Engel and J. Ranft, Phys. Rev. **D54** (1996) 4244.

[25] A. Buijs et al., Comp. Phys. Comm. **79** (1994) 523.

[26] OPAL Collab. K. Ackerstaff et al., Z. Phys. **C74** (1997) 33.

[27] J. Fujimoto et al., Comp. Phys. Comm. **100** (1997) 128.

[28] F.A. Berends, R. Pittau and R. Kleiss, Comp. Phys. Comm. **85** (1995) 437.

[29] OPAL Collab., G. Abbiendi et al., *Multi-photon production in* e$^+$e$^-$ *collisions at* $\sqrt{s} = $ *189 GeV*, CERN-EP/99-088, submitted to Phys. Lett. B.

[30] The LEP Working Group for Higgs Boson Searches, ALEPH, DELPHI, L3 and OPAL Collaborations, *Limits on Higgs Boson Masses from Combining the Data of the Four LEP Experiments at Energies up to 183 GeV*, CERN-EP/99-060.

[31] The LEP Electroweak Working Group and the SLD Heavy Flavour and Electroweak Groups, ALEPH, DELPHI, L3, OPAL and SLD Collaborations, *A Combination of Preliminary Electroweak Measurements and Constraints on the Standard Model*, CERN-EP/99-015.

[32] G. Montagna, O. Nicrosini, G. Passarino, F. Piccinini and R.Pittau, Comp. Phys. Comm. **76** (1993) 328;
G. Montagna, O. Nicrosini, G. Passarino and F. Piccinini, Comp. Phys. Comm. **93** (1996) 120;
G. Montagna, O. Nicrosini, F. Piccinini and G. Passarino, hep-ph/9804211.
We use TOPAZ0 version 4.4 with default parameters, except `ONP='Y'`, and with the same input parameters as for ZFITTER.

[33] S. Jadach, W. Placzek, B.F.L. Ward, Phys. Lett. **B390** (1997) 298.

[34] D. Bardin et al., Nucl. Phys. Proc. Suppl. **37B** (1994) 148.

[35] J. Hilgart, R. Kleiss, F. Le Diberder, Comp. Phys. Comm. **75** (1993) 191.

[36] HRS Collab., D. Bender et al., Phys. Rev. **D31** (1985) 1;
MAC Collab., E. Fernandez et al., Phys. Rev. **D31** (1985) 1537;
PLUTO Collab., C. Berger et al., Phys. Lett. **B81** (1979) 410;
CELLO Collab., H.J. Behrend et al., Phys. Lett. **B183** (1987) 400;
JADE Collab., W. Bartel et al., Phys. Lett. **B129** (1983) 145;
JADE Collab., W. Bartel et al., Phys. Lett. **B160** (1985) 337;
MARKJ Collab., B. Adeva et al., Phys. Rev. Lett. **50** (1983) 799;
MARKJ Collab., B. Adeva et al., Phys. Rev. **D34** (1986) 681;
TASSO Collab., R. Brandelik et al., Phys. Lett. **B113** (1982) 499;
TASSO Collab., M. Althoff et al., Phys. Lett. **B138** (1984) 441;
AMY Collab., T. Mori et al., Phys. Lett. **B218** (1989) 499;
TOPAZ Collab., I. Adachi et al., Phys. Rev. Lett. **60** (1988) 97;
VENUS Collab., H. Yoshida et al., Phys. Lett. **B198** (1987) 570;
TOPAZ Collab., K. Miyabayashi et al., Phys. Lett. **B347** (1995) 171.

[37] TOPAZ Collab., I. Levine et al., Phys. Rev. Lett. **78** (1997) 424.

[38] M. Kobel, *Direct Measurements of the Electromagnetic Coupling Constant at Large q^2*, FREIBURG-EHEP 97-13, Contributed paper to the XVIII International Symposium on Lepton Photon Interactions, Hamburg, July 1997.

[39] M.E. Cage et al., IEEE Trans. Instrum. Meth. **38** (1989) 284.

[40] E. Eichten, K. Lane, M. Peskin, Phys. Rev. Lett. **50** (1983) 811.

[41] See for example *Contact interactions and new heavy bosons at HERA: a model independent analysis*, P. Haberl, F. Schrempp, H.U. Martyn, in Proceedings, Physics at HERA, **vol. 2**, (1991) 1133.

[42] OPAL Collab., G. Alexander et al., Phys. Lett. **B387** (1996) 432.

[43] G.J. Gounaris, D.T. Papadamou, F.M. Renard, Phys. Rev. **D56** (1997) 3970.

[44] CDF Collab., F. Abe et al., Phys. Rev. Lett. **79** (1997) 2198.

[45] H1 Collab., S. Aid et al., Phys. Lett. **B353** (1995) 578.

[46] A. Deandrea, Phys. Lett. **B409** (1997) 277.

[47] J. Wess, J. Bagger, *Supersymmetry and Supergravity* (Princeton University Press, 1983);
H.P. Nilles, Phys. Rep. **110** (1984) 1;
H.E. Haber, G.E. Kane, Phys. Rep. **117** (1985) 75;
R. Barbieri, Riv. Nuovo Cim. **11** (1988) 1;
P. West, *Introduction to Supersymmetry and Supergravity* (World Scientific, 1986).

[48] J. Kalinowski, R. Rückl, H. Spiesberger, P.M. Zerwas, Phys. Lett. **B406** (1997) 314.

[49] ALEPH Collab., R. Barate et al., Eur. Phys. J. **C4** (1998) 433;
OPAL Collab., G. Abbiendi et al., *Search for R-parity Violating Decays of Scalar Fermions at LEP*, CERN-EP/99-043, submitted to Eur. Phys. J. C.

[50] J.L. Hewett, Phys. Rev. Lett. **82** (1999) 4765.

[51] E.A. Mirabelli, M. Perelstein, M.E. Peskin, Phys. Rev. Lett. **82** (1999) 2236.

[52] T.G. Rizzo, Phys. Rev. **D59** (1999) 115010.

[53] F.A. Berends and R. Kleiss, Nucl. Phys. **B186** (1981) 22.

19

Efficiencies and backgrounds at $\sqrt{s} = 189$ GeV				
Channel		Efficiency (%)	Background (pb)	Feedthrough (pb)
$q\overline{q}X$		90.3±0.5	4.2±0.9	–
$q\overline{q}$	$s'/s > 0.01$	87.3±0.5	6.5±0.9	–
	$s'/s > 0.7225$	87.7±0.7	1.55±0.09	1.1±0.1
e^+e^-	$\lvert\cos\theta\rvert < 0.9$, $\theta_{\mathrm{acol}} < 170°$	97.8±0.6	1.57±0.09	–
	$\lvert\cos\theta_{\mathrm{e}^-}\rvert < 0.7$, $\theta_{\mathrm{acol}} < 10°$	98.9±0.4	0.25±0.03	–
	$\lvert\cos\theta\rvert < 0.96$, $\theta_{\mathrm{acol}} < 10°$	98.5±0.4	10.4±0.4	–
$\mu^+\mu^-$	$s'/s > 0.01$	75.4±0.8	0.39±0.11	–
	$s'/s > 0.7225$	88.7±0.9	0.07±0.03	0.060±0.003
$\tau^+\tau^-$	$s'/s > 0.01$	40.2±1.0	0.54±0.10	–
	$s'/s > 0.7225$	58.3±1.5	0.17±0.03	0.072±0.003

Table 1: Efficiency of selection cuts, background and feedthrough of events with lower s' into the non-radiative samples for each channel at 189 GeV. The errors include Monte Carlo statistics and systematic effects. In the case of electron pairs, the efficiencies are effective values including the efficiency of selection cuts for events within the acceptance region and the effect of acceptance corrections. An acceptance of $\lvert\cos\theta\rvert < 0.9$ (or 0.96) means that both electron and positron must satisfy this cut, whereas $\lvert\cos\theta_{\mathrm{e}^-}\rvert < 0.7$ means that only the electron need do so.

Cross-sections at $\sqrt{s} = 189$ GeV					
Channel		$\int \mathcal{L}\mathrm{d}t$ (pb^{-1})	Events	σ (pb)	σ^{SM} (pb)
q$\bar{\mathrm{q}}$X		185.6	20025	114.8±0.9 ±1.2	114.3
q$\bar{\mathrm{q}}$	$s'/s > 0.01$	185.6	17228	99.5±0.8 ±1.2	98.8
	$s'/s > 0.7225$		4072	22.10±0.37±0.24	22.16
e$^+$e$^-$	$\lvert\cos\theta\rvert < 0.9,\ \theta_{\mathrm{acol}} < 170°$	185.8	20487	111.2±0.8 ±0.7	112.0
	$\lvert\cos\theta_{\mathrm{e}^-}\rvert < 0.7,\ \theta_{\mathrm{acol}} < 10°$		3735	20.08±0.33±0.10	20.39
	$\lvert\cos\theta\rvert < 0.96,\ \theta_{\mathrm{acol}} < 10°$		57685	304.6±1.3 ±1.4	311.6
$\mu^+\mu^-$	$s'/s > 0.01$	180.0	1129	7.77±0.23±0.18	7.76
	$s'/s > 0.7225$		527	3.11±0.14±0.06	3.21
$\tau^+\tau^-$	$s'/s > 0.01$	180.6	730	8.67±0.32±0.34	7.75
	$s'/s > 0.7225$		420	3.54±0.17±0.11	3.21

Table 2: Integrated luminosity used in the analysis, numbers of selected events and measured cross-sections at $\sqrt{s}$=188.63 GeV. For the cross-sections, the first error shown is statistical, the second systematic. As in [1, 2], the cross-sections for hadrons, $\mu^+\mu^-$ and $\tau^+\tau^-$ are defined to cover phase-space up to the limit imposed by the s'/s cut, with $\sqrt{s'}$ defined as the invariant mass of the outgoing two-fermion system *before* final-state photon radiation. The contribution of interference between initial- and final-state radiation has been removed. The last column shows the Standard Model cross-section predictions from ZFITTER [15] (hadrons, $\mu^+\mu^-$, $\tau^+\tau^-$) and ALIBABA [16] (e$^+$e$^-$).

Asymmetries at $\sqrt{s} = 189$ GeV					
		N_{F}	N_{B}	A_{FB}	$A_{\mathrm{FB}}^{\mathrm{SM}}$
e$^+$e$^-$	$\lvert\cos\theta_{\mathrm{e}^-}\rvert < 0.7$ and $\theta_{\mathrm{acol}} < 10°$	3318	349	0.814±0.010±0.005	0.813
$\mu^+\mu^-$	$s'/s > 0.01$	682	372	0.253±0.031±0.003	0.277
	$s'/s > 0.7225$	370	115.5	0.532±0.042±0.007	0.566
$\tau^+\tau^-$	$s'/s > 0.01$	485	217	0.315±0.042±0.003	0.278
	$s'/s > 0.7225$	316.5	89.5	0.606±0.048±0.007	0.566
Combined	$s'/s > 0.01$			0.277±0.025±0.002	0.277
$\mu^+\mu^-$ and $\tau^+\tau^-$	$s'/s > 0.7225$			0.563±0.031±0.005	0.566

Table 3: The numbers of forward (N_{F}) and backward (N_{B}) events and measured asymmetry values at 188.63 GeV. The measured asymmetry values include corrections for background and efficiency, and in the case of muons and taus are corrected to the full solid angle. The first error is statistical and the second systematic. The asymmetries for $\mu^+\mu^-$, $\tau^+\tau^-$ and for the combined $\mu^+\mu^-$ and $\tau^+\tau^-$ are shown after the correction for interference between initial- and final-state radiation. The final column shows the Standard Model predictions of ALIBABA for e$^+$e$^-$ and ZFITTER for the other final states.

Hadrons at $\sqrt{s} = 189$ GeV	
$\lvert\cos\theta\rvert$	$\mathrm{d}\sigma/\mathrm{d}\lvert\cos\theta\rvert$ (pb)
$[0.0, 0.1]$	17.5±1.0
$[0.1, 0.2]$	17.7±1.1
$[0.2, 0.3]$	16.8±1.0
$[0.3, 0.4]$	18.2±1.1
$[0.4, 0.5]$	18.8±1.1
$[0.5, 0.6]$	21.6±1.2
$[0.6, 0.7]$	24.2±1.2
$[0.7, 0.8]$	26.0±1.3
$[0.8, 0.9]$	27.7±1.3
$[0.9, 1.0]$	31.4±1.7

Table 4: Differential cross-section for q$\overline{\mathrm{q}}$ production, for $s'/s > 0.7225$. The values are corrected to no interference between initial- and final-state radiation as in [2]. Errors include statistical and systematic effects combined, with the former dominant.

e$^+$e$^-$ at $\sqrt{s} = 189$ GeV		
$\cos\theta$		$\mathrm{d}\sigma/\mathrm{d}\cos\theta$ (pb)
$[-0.9,$	$-0.7]$	1.4±0.2
$[-0.7,$	$-0.5]$	2.0±0.2
$[-0.5,$	$-0.3]$	2.4±0.3
$[-0.3,$	$-0.1]$	3.0±0.3
$[-0.1,$	$0.1]$	4.3±0.3
$[\ \ 0.1,$	$0.3]$	8.3±0.5
$[\ \ 0.3,$	$0.5]$	19.3±0.7
$[\ \ 0.5,$	$0.7]$	61.4±1.4
$[\ \ 0.7,$	$0.9]$	415±5

Table 5: Differential cross-section for electron pair production for $\theta_{\mathrm{acol}} < 10°$. Errors include statistical and systematic effects combined.

$\mu^+\mu^-$ at $\sqrt{s} = 189$ GeV	
$\cos\theta$	$\mathrm{d}\sigma/\mathrm{dcos}\,\theta$ (pb)
$[-1.0, -0.8]$	$0.67\pm^{0.21}_{0.17}$
$[-0.8, -0.6]$	$0.36\pm^{0.14}_{0.11}$
$[-0.6, -0.4]$	$0.50\pm^{0.16}_{0.13}$
$[-0.4, -0.2]$	0.66 ± 0.14
$[-0.2, \ \ 0.0]$	1.33 ± 0.20
$[\ \ 0.0, \ \ 0.2]$	1.20 ± 0.19
$[\ \ 0.2, \ \ 0.4]$	1.85 ± 0.24
$[\ \ 0.4, \ \ 0.6]$	2.04 ± 0.27
$[\ \ 0.6, \ \ 0.8]$	2.64 ± 0.30
$[\ \ 0.8, \ \ 1.0]$	3.96 ± 0.43
$\tau^+\tau^-$ at $\sqrt{s} = 189$ GeV	
$\cos\theta$	$\mathrm{d}\sigma/\mathrm{dcos}\,\theta$ (pb)
$[-1.0, -0.8]$	$0.99\pm^{0.44}_{0.33}$
$[-0.8, -0.6]$	$0.39\pm^{0.19}_{0.15}$
$[-0.6, -0.4]$	0.75 ± 0.18
$[-0.4, -0.2]$	0.76 ± 0.18
$[-0.2, \ \ 0.0]$	0.84 ± 0.19
$[\ \ 0.0, \ \ 0.2]$	1.68 ± 0.27
$[\ \ 0.2, \ \ 0.4]$	2.00 ± 0.30
$[\ \ 0.4, \ \ 0.6]$	2.52 ± 0.33
$[\ \ 0.6, \ \ 0.8]$	3.29 ± 0.40
$[\ \ 0.8, \ \ 1.0]$	5.1 ± 0.8

Table 6: Differential cross-sections for $\mu^+\mu^-$ and $\tau^+\tau^-$ pair production. The values are for $s'/s > 0.7225$ and are corrected to no interference between initial- and final-state radiation. Errors include statistical and systematic effects combined, with the former dominant.

Interference Corrections at $\sqrt{s} = 189$ GeV		
	$s'/s > 0.01$	$s'/s > 0.7225$
$\Delta\sigma/\sigma_{\mathrm{SM}}$(had) (%)	$+0.05 \pm 0.00 \pm 0.05$	$+0.4 \pm 0.1 \pm 0.2$
$\Delta\sigma/\sigma_{\mathrm{SM}}(\mu\mu)$ (%)	-0.42 ± 0.05	-1.4 ± 0.4
$\Delta\sigma/\sigma_{\mathrm{SM}}(\tau\tau)$ (%)	-0.48 ± 0.06	-1.2 ± 0.3
$\Delta A_{\mathrm{FB}}(\mu\mu)$	-0.0054 ± 0.0007	-0.016 ± 0.004
$\Delta A_{\mathrm{FB}}(\tau\tau)$	-0.0053 ± 0.0009	-0.012 ± 0.003
ΔA_{FB}(combined)	-0.0056 ± 0.0006	-0.014 ± 0.003

Table 7: Corrections $\Delta\sigma$ and ΔA_{FB} which have been applied to the measured cross-sections and asymmetries in order to remove the contribution from interference between initial- and final-state radiation. Cross-section corrections are expressed as a fraction of the expected Standard Model cross-section, while asymmetry corrections are given as absolute numbers, and depend on the observed asymmetry. The first error reflects the uncertainty from modelling the selection efficiency for the interference cross-section, and is very small for hadrons because the efficiency is large and depends only weakly on $\cos\theta$. The second error is our estimate of possible additional QCD corrections for the hadrons [2].

	$s'/s > 0.01$	$s'/s > 0.7225$
MC statistics (efficiency)	0.05	0.14
MC statistics (background)	0.27	0.14
ISR modelling	0.45	0.48
Fragmentation modelling	0.34	0.32
Detector effects	0.19	0.42
s' determination	–	0.30
WW rejection cuts	0.11	0.52
WW background	0.15	0.39
Background	0.98	0.09
Interference	0.05	0.22
Luminosity	0.21	0.21
Total	1.2	1.1

Table 8: Systematic errors, in %, on the hadronic cross-section measurements.

	$|\cos\theta_{e^\pm}| < 0.9$	$|\cos\theta_{e^-}| < 0.7$	$|\cos\theta_{e^\pm}| < 0.96$
	$\theta_{\text{acol}} < 170°$	$\theta_{\text{acol}} < 10°$	$\theta_{\text{acol}} < 10°$
MC statistics	0.05	0.10	0.05
Four-fermion contribution	0.03	0.06	0.01
Multiplicity cuts	0.12	0.05	0.03
Calorimeter energy scale/resolution	0.01	0.01	0.10
Track requirements	0.42	0.38	–
Acceptance correction	0.37	0.19	0.37
Background	0.08	0.15	0.12
Luminosity	0.21	0.21	0.21
Total	0.6	0.5	0.5

Table 9: Systematic errors, in %, on the electron pair cross-section measurements.

	$s'/s > 0.01$	$s'/s > 0.7225$
MC statistics (efficiency)	0.2	0.2
MC statistics (background)	0.2	0.2
MC statistics (feedthrough)	–	0.1
Efficiency	1.0	1.0
Cosmic background	0.5	1.0
Other background	1.9	1.1
Feedthrough	–	0.1
Interference	<0.1	0.4
Luminosity	0.2	0.2
Total	2.3	1.8

Table 10: Systematic errors, in %, on the muon pair cross-section measurements.

	$s'/s > 0.01$	$s'/s > 0.7225$
MC statistics (efficiency)	0.4	0.5
MC statistics (background)	0.6	0.5
MC statistics (feedthrough)	–	0.1
Efficiency	2.5	2.5
Background	2.9	1.5
Feedthrough	–	0.1
Interference	0.1	0.3
Luminosity	0.2	0.2
Total	3.9	3.0

Table 11: Systematic errors, in %, on the tau pair cross-section measurements.

$\sqrt{s}$ (GeV)	Fit		Standard Model	
	$1/\alpha_{\mathrm{em}}$	χ^2/d.o.f.	$1/\alpha_{\mathrm{em}}$	χ^2/d.o.f.
188.63	$126.2^{+3.7}_{-3.2}$	3.0/3	127.8	3.2/4
181.94	$126.8^{+3.0}_{-2.7}$	15.0/23	127.9	15.2/24

Table 12: Results of fits for α_{em}. The first row shows the fit to data at 188.63 GeV, the second row the combined fit to these data and measurements at 130–183 GeV [1,2]. For the combined fit, the value of α_{em} is quoted at the centre-of-mass energy corresponding to the luminosity-weighted average of $1/s$. The errors on the fitted values of α_{em} arise from the errors on the measurements; errors due to uncertainties in the ZFITTER input parameters are negligible. The Standard Model values of $1/\alpha_{\mathrm{em}}$, and the χ^2 between the measurements and the Standard Model predictions are also given for comparison.

Table 13: Results of the contact interaction fits to the angular distributions for non-radiative $e^+e^- \to e^+e^-$, $e^+e^- \to \mu^+\mu^-$, $e^+e^- \to \tau^+\tau^-$ and the cross-sections for $e^+e^- \to q\bar{q}$. Results at centre-of-mass energies of 130–183 GeV [2,1] are also included. The combined results include all leptonic angular distributions and the hadronic cross-sections. The numbers in square brackets are the values of $[\eta_{LL}, \eta_{RR}, \eta_{LR}, \eta_{RL}]$ which define the models. Note that the values of η for the $\overline{\mathcal{O}}_{DB}$ model [43] have been scaled down by a factor of 4 compared with those used in [1]. ε_0 is the fitted value of $\varepsilon = 1/\Lambda^2$, $\Lambda_{\pm}$ are the 95% confidence level limits. The units of Λ are TeV, those of ε_0 are TeV^{-2}.

Channel		LL	RR	LR	RL	VV	AA	LL+RR	LR+RL	$\overline{\mathcal{O}}_{DB}$
		$[\pm1,0,0,0]$	$[0,\pm1,0,0]$	$[0,0,\pm1,0]$	$[0,0,0,\pm1]$	$[\pm1,\pm1,\pm1,\pm1]$	$[\pm1,\pm1,\mp1,\mp1]$	$[\pm1,\pm1,0,0]$	$[0,0,\pm1,\pm1]$	$[\pm\frac{1}{4},\pm1,\pm\frac{1}{2},\pm\frac{1}{2}]$
e^+e^-	ε_0	$0.016^{+0.026}_{-0.024}$	$0.016^{+0.026}_{-0.024}$	$0.008^{+0.013}_{-0.013}$	$0.008^{+0.013}_{-0.013}$	$0.003^{+0.005}_{-0.005}$	$-0.002^{+0.008}_{-0.008}$	$0.008^{+0.012}_{-0.012}$	$0.004^{+0.007}_{-0.007}$	$0.006^{+0.009}_{-0.009}$
	Λ_+	3.8	3.8	5.3	5.3	8.9	8.9	5.5	7.7	6.5
	Λ_-	5.6	5.5	7.5	7.5	12.4	7.2	7.7	10.4	9.1
$\mu^+\mu^-$	ε_0	$-0.015^{+0.015}_{-0.016}$	$-0.018^{+0.018}_{-0.017}$	$-0.003^{+0.018}_{-0.021}$	$-0.003^{+0.018}_{-0.021}$	$-0.005^{+0.006}_{-0.006}$	$-0.005^{+0.007}_{-0.007}$	$-0.008^{+0.008}_{-0.008}$	$-0.002^{+0.010}_{-0.009}$	$-0.009^{+0.010}_{-0.010}$
	Λ_+	7.3	7.0	5.5	5.5	11.3	10.3	10.0	7.6	8.6
	Λ_-	4.6	4.4	1.9	1.9	7.9	7.5	6.5	7.0	5.8
$\tau^+\tau^-$	ε_0	$0.024^{+0.021}_{-0.020}$	$0.027^{+0.022}_{-0.023}$	$-0.239^{+0.034}_{-0.031}$	$-0.239^{+0.034}_{-0.031}$	$0.005^{+0.008}_{-0.008}$	$0.011^{+0.009}_{-0.009}$	$0.013^{+0.011}_{-0.011}$	$-0.244^{+0.016}_{-0.016}$	$0.010^{+0.014}_{-0.014}$
	Λ_+	3.9	3.8	5.0	5.0	6.9	5.9	5.3	6.8	5.1
	Λ_-	6.5	6.2	1.9	1.9	9.5	10.0	9.1	1.9	7.2
$\ell^+\ell^-$	ε_0	$0.002^{+0.011}_{-0.011}$	$0.003^{+0.012}_{-0.012}$	$0.002^{+0.010}_{-0.010}$	$0.002^{+0.010}_{-0.010}$	$0.001^{+0.003}_{-0.003}$	$0.000^{+0.004}_{-0.004}$	$0.001^{+0.006}_{-0.006}$	$0.001^{+0.005}_{-0.005}$	$0.002^{+0.006}_{-0.006}$
	Λ_+	6.4	6.2	6.8	6.8	11.5	10.9	8.9	9.5	8.5
	Λ_-	7.2	7.0	7.7	7.7	13.4	10.6	10.1	10.9	9.9
$q\bar{q}$	ε_0	$-0.064^{+0.080}_{-0.026}$	$0.029^{+0.036}_{-0.052}$	$0.008^{+0.041}_{-0.041}$	$0.111^{+0.018}_{-0.027}$	$0.021^{+0.016}_{-0.031}$	$-0.037^{+0.044}_{-0.013}$	$-0.012^{+0.032}_{-0.025}$	$0.062^{+0.015}_{-0.072}$	$0.070^{+0.016}_{-0.079}$
	Λ_+	5.5	3.5	3.8	2.7	4.7	8.1	5.4	3.4	3.2
	Λ_-	3.1	4.9	4.4	6.4	7.2	4.2	4.4	7.1	6.7
combined	ε_0	$0.001^{+0.010}_{-0.010}$	$0.003^{+0.010}_{-0.010}$	$0.003^{+0.010}_{-0.010}$	$0.003^{+0.009}_{-0.008}$	$0.001^{+0.003}_{-0.003}$	$-0.001^{+0.004}_{-0.004}$	$0.001^{+0.006}_{-0.006}$	$0.002^{+0.005}_{-0.005}$	$0.002^{+0.006}_{-0.006}$
	Λ_+	7.1	6.8	6.8	6.9	11.4	11.6	9.0	9.5	8.5
	Λ_-	7.2	7.4	7.8	8.6	13.7	10.5	10.0	11.4	10.5
$u\bar{u}$	ε_0	$0.005^{+0.018}_{-0.017}$	$0.009^{+0.027}_{-0.025}$	$0.144^{+0.056}_{-0.182}$	$0.000^{+0.103}_{-0.076}$	$0.002^{+0.009}_{-0.008}$	$0.004^{+0.014}_{-0.012}$	$0.003^{+0.011}_{-0.010}$	$0.012^{+0.113}_{-0.043}$	$0.004^{+0.019}_{-0.016}$
	Λ_+	4.9	1.5	2.1	2.6	7.0	5.4	6.4	2.5	4.9
	Λ_-	6.1	5.1	3.7	2.9	8.6	7.3	7.8	4.2	6.1
$d\bar{d}$	ε_0	$-0.007^{+0.020}_{-0.021}$	$-0.191^{+0.221}_{-0.050}$	$-0.042^{+0.098}_{-0.095}$	$0.152^{+0.058}_{-0.184}$	$-0.005^{+0.015}_{-0.020}$	$-0.004^{+0.012}_{-0.014}$	$-0.004^{+0.014}_{-0.015}$	$0.040^{+0.051}_{-0.078}$	$-0.123^{+0.152}_{-0.044}$
	Λ_+	5.7	4.0	3.2	2.0	6.5	7.3	6.7	2.9	4.2
	Λ_-	4.5	1.9	2.4	3.8	2.3	5.4	5.3	3.7	2.3
$u\bar{u}+d\bar{d}$	ε_0	$0.021^{+0.065}_{-0.066}$	$0.090^{+0.043}_{-0.115}$	$0.021^{+0.065}_{-0.066}$	$0.091^{+0.044}_{-0.118}$	$0.068^{+0.016}_{-0.078}$	$0.000^{+0.031}_{-0.032}$	$0.063^{+0.031}_{-0.082}$	$0.063^{+0.031}_{-0.083}$	$0.122^{+0.023}_{-0.052}$
	Λ_+	2.9	2.5	2.9	2.5	3.2	4.6	3.0	3.0	2.5
	Λ_-	3.6	4.3	3.6	4.3	6.6	4.6	5.0	5.0	5.4

Processes	$\sqrt{s}$ [GeV]	λ	M_{s} [TeV] (95% C.L.)
$\mathrm{e^+e^-} \to \mu^+\mu^-$	183,189	$+1$	0.60
		-1	0.63
$\mathrm{e^+e^-} \to \tau^+\tau^-$	183,189	$+1$	0.63
		-1	0.50
$\mathrm{e^+e^-} \to \mu^+\mu^-, \tau^+\tau^-$	183,189	$+1$	0.68
		-1	0.61

Table 14: Lower limits on M_{s} at 95% confidence level.

OPAL 189 GeV
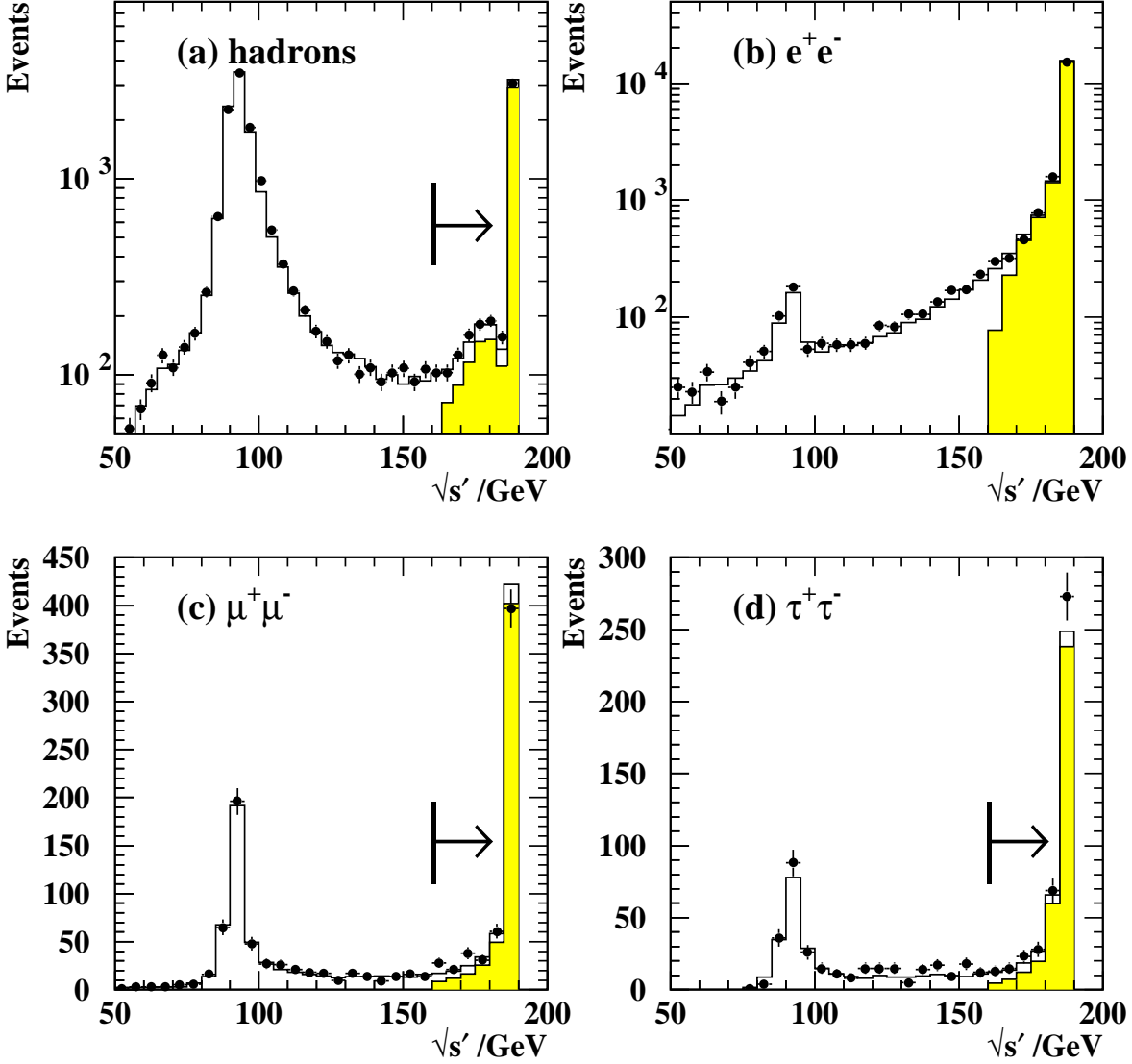
Figure 1: The distributions of reconstructed $\sqrt{s'}$ for (a) hadronic events, (b) electron pair events with $|\cos\theta_{e^+}| < 0.9$, $|\cos\theta_{e^-}| < 0.9$ and $\theta_{acol} < 170°$, (c) muon pair and (d) tau pair events at 188.63 GeV. In each case, the points show the data and the histogram the Monte Carlo prediction, normalized to the integrated luminosity of the data, with the contribution from events with true $s'/s > 0.7225$ shaded in (a), (c) and (d), and the contribution from events with $\theta_{acol} < 10°$ shaded in (b). The arrows in (a), (c) and (d) show the position of the cut used to select 'non-radiative' events.
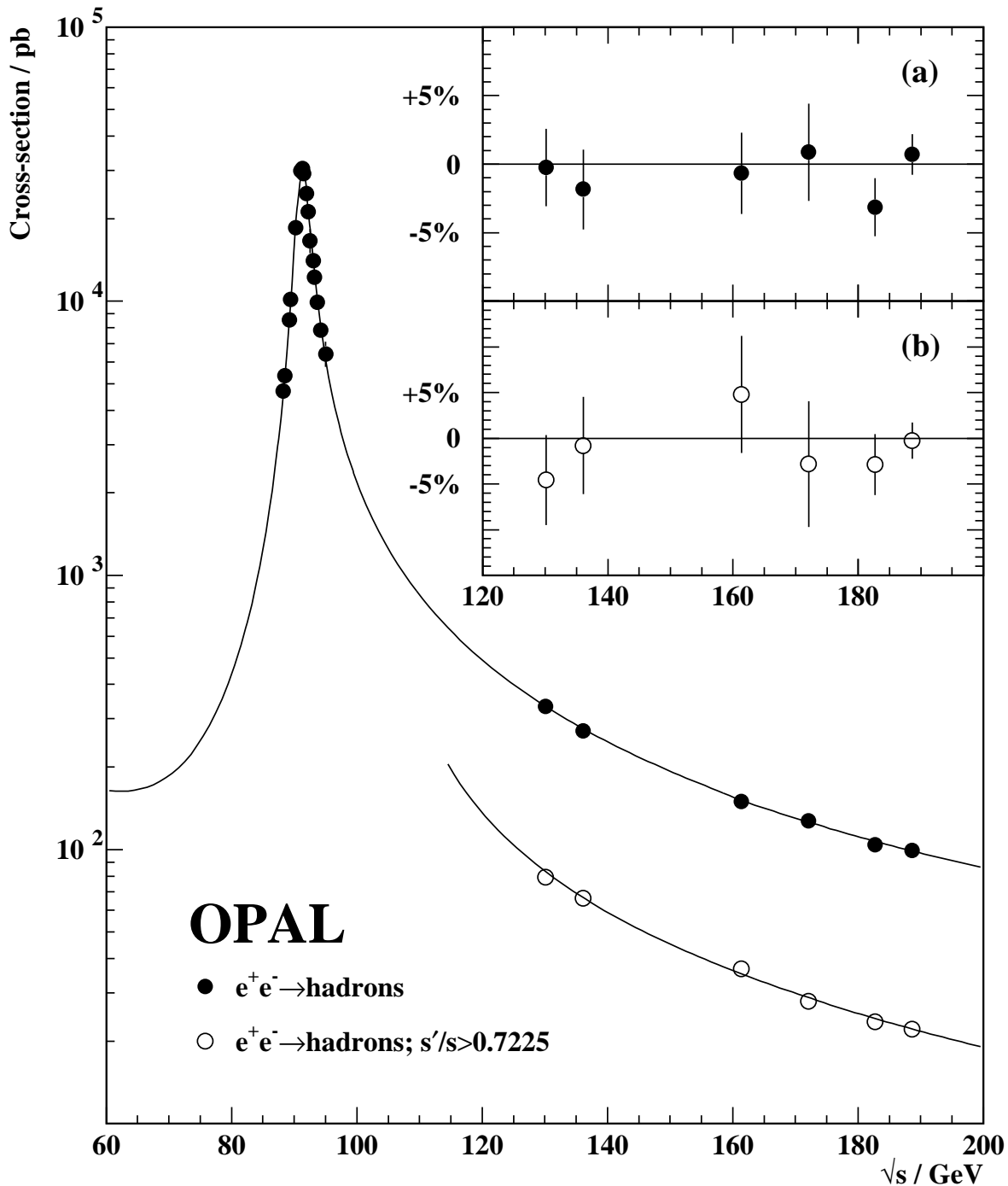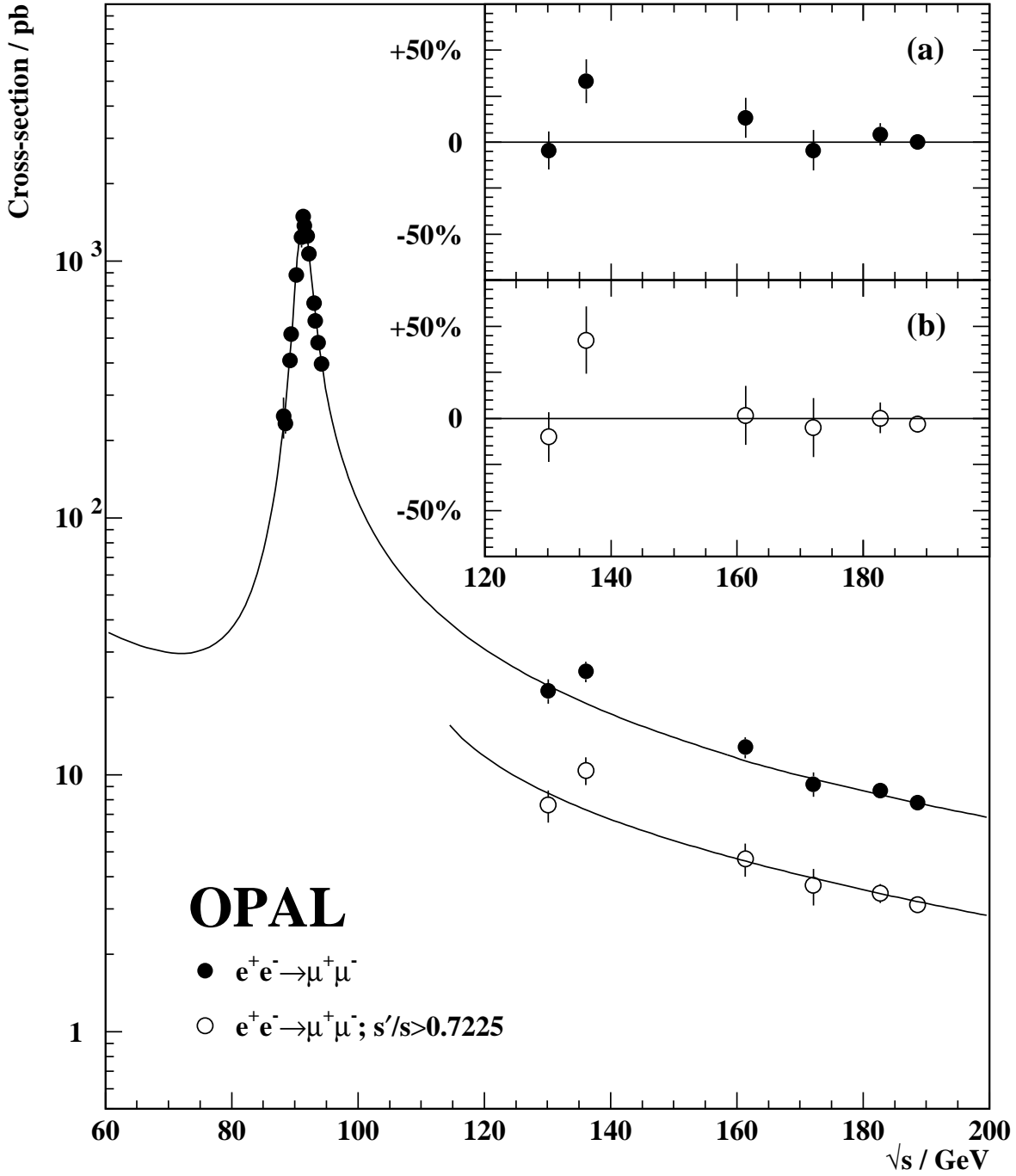
Figure 2: Measured total cross-sections ($s'/s > 0.01$) for hadronic events at lower energies [19, 17, 18, 2, 1], and this analysis. Cross-section measurements for $s'/s > 0.7225$ from this analysis and from [2, 1] are also shown; where necessary, the latter have been corrected from $s'/s > 0.8$ to $s'/s > 0.7225$ by adding the prediction of ZFITTER for this difference before plotting. The curves show the predictions of ZFITTER. The insets show the percentage differences between the measured values and the ZFITTER predictions for the high energy points for (a) $s'/s > 0.01$ and (b) $s'/s > 0.7225$.
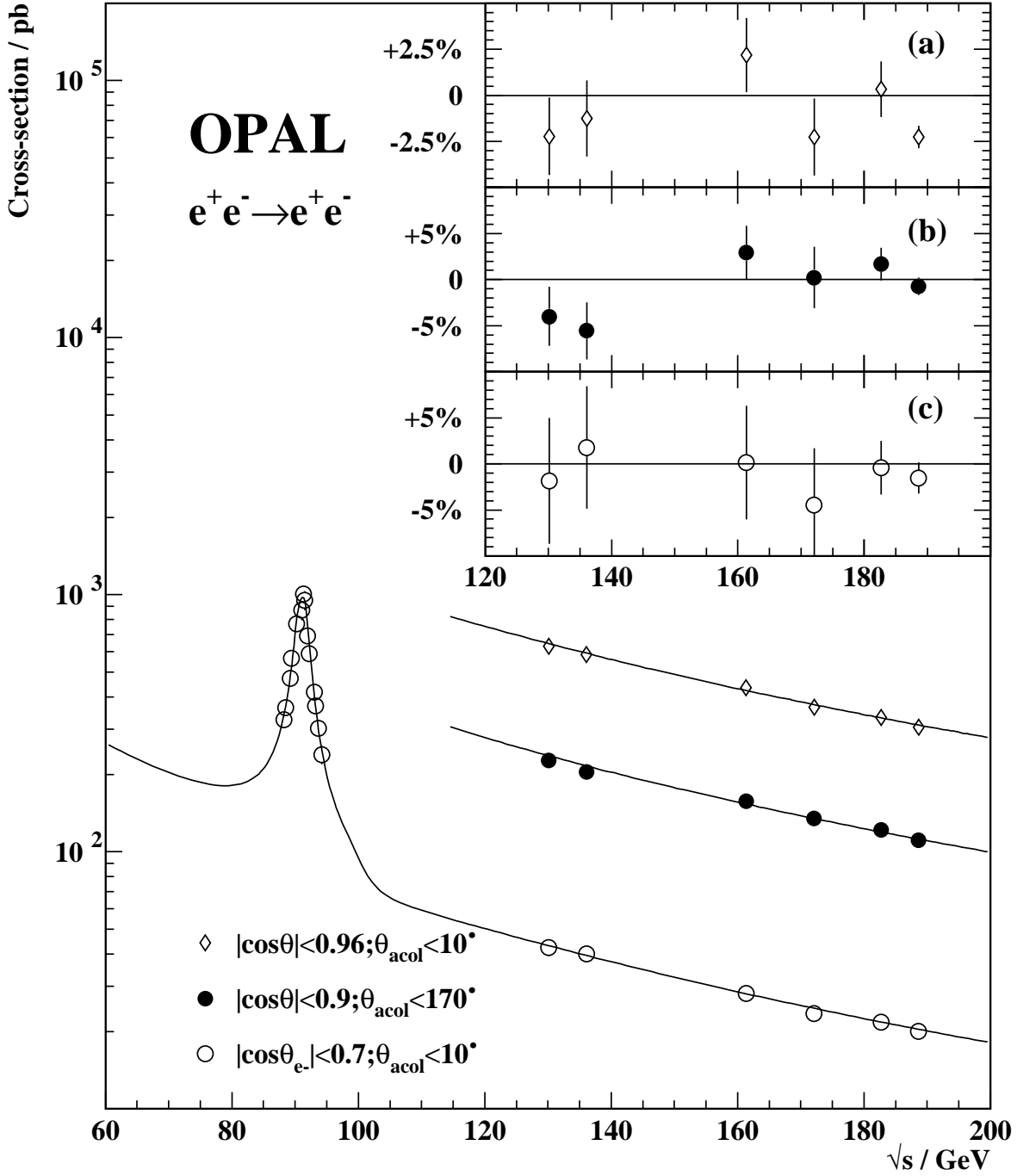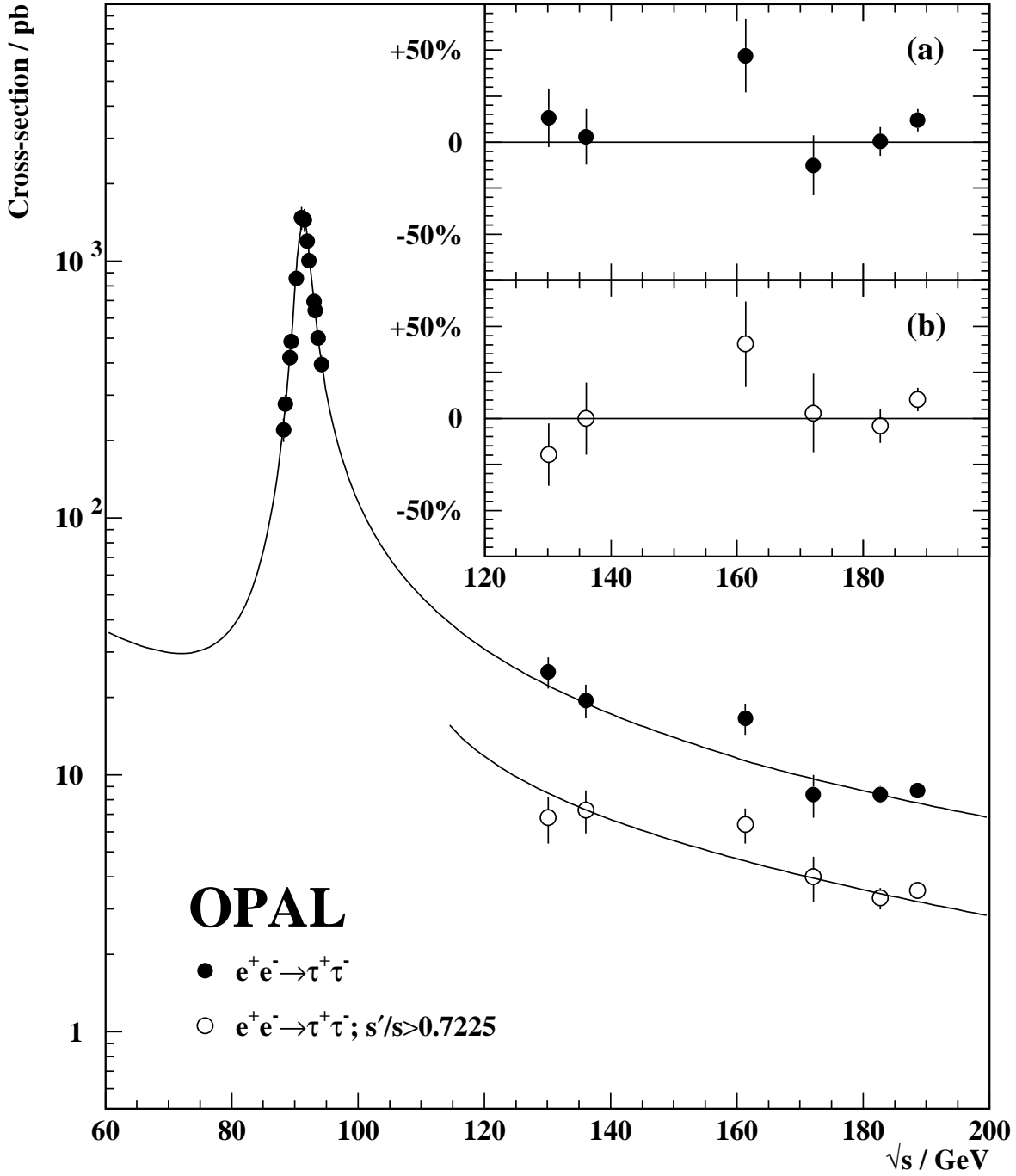
Figure 3: Measured cross-sections for electron pair events at lower energies [19, 17, 18, 2, 1], and this analysis. The curves show the predictions of ALIBABA. The insets show the percentage differences between the measured values and the ALIBABA predictions for the high energy points for (a) $|\cos\theta| < 0.96$, $\theta_{\mathrm{acol}} < 10°$, (b) $|\cos\theta| < 0.9$, $\theta_{\mathrm{acol}} < 170°$ and (c) $|\cos\theta_{\mathrm{e^-}}| < 0.7$, $\theta_{\mathrm{acol}} < 10°$.

Figure 4: Measured total cross-sections ($s'/s > 0.01$) for muon pair events at lower energies [19, 17, 18, 2, 1], and this analysis. Cross-section measurements for $s'/s > 0.7225$ from this analysis and from [2, 1] are also shown; where necessary, the latter have been corrected from $s'/s > 0.8$ to $s'/s > 0.7225$ by adding the prediction of ZFITTER for this difference before plotting. The curves show the predictions of ZFITTER. The insets show the percentage differences between the measured values and the ZFITTER predictions for the high energy points for (a) $s'/s > 0.01$ and (b) $s'/s > 0.7225$.

Figure 5: Measured total cross-sections ($s'/s > 0.01$) for tau pair events at lower energies [19, 17, 18, 2, 1], and this analysis. Cross-section measurements for $s'/s > 0.7225$ from this analysis and from [2, 1] are also shown; where necessary, the latter have been corrected from $s'/s > 0.8$ to $s'/s > 0.7225$ by adding the prediction of ZFITTER for this difference before plotting. The curves show the predictions of ZFITTER. The insets show the percentage differences between the measured values and the ZFITTER predictions for the high energy points for (a) $s'/s > 0.01$ and (b) $s'/s > 0.7225$.

33
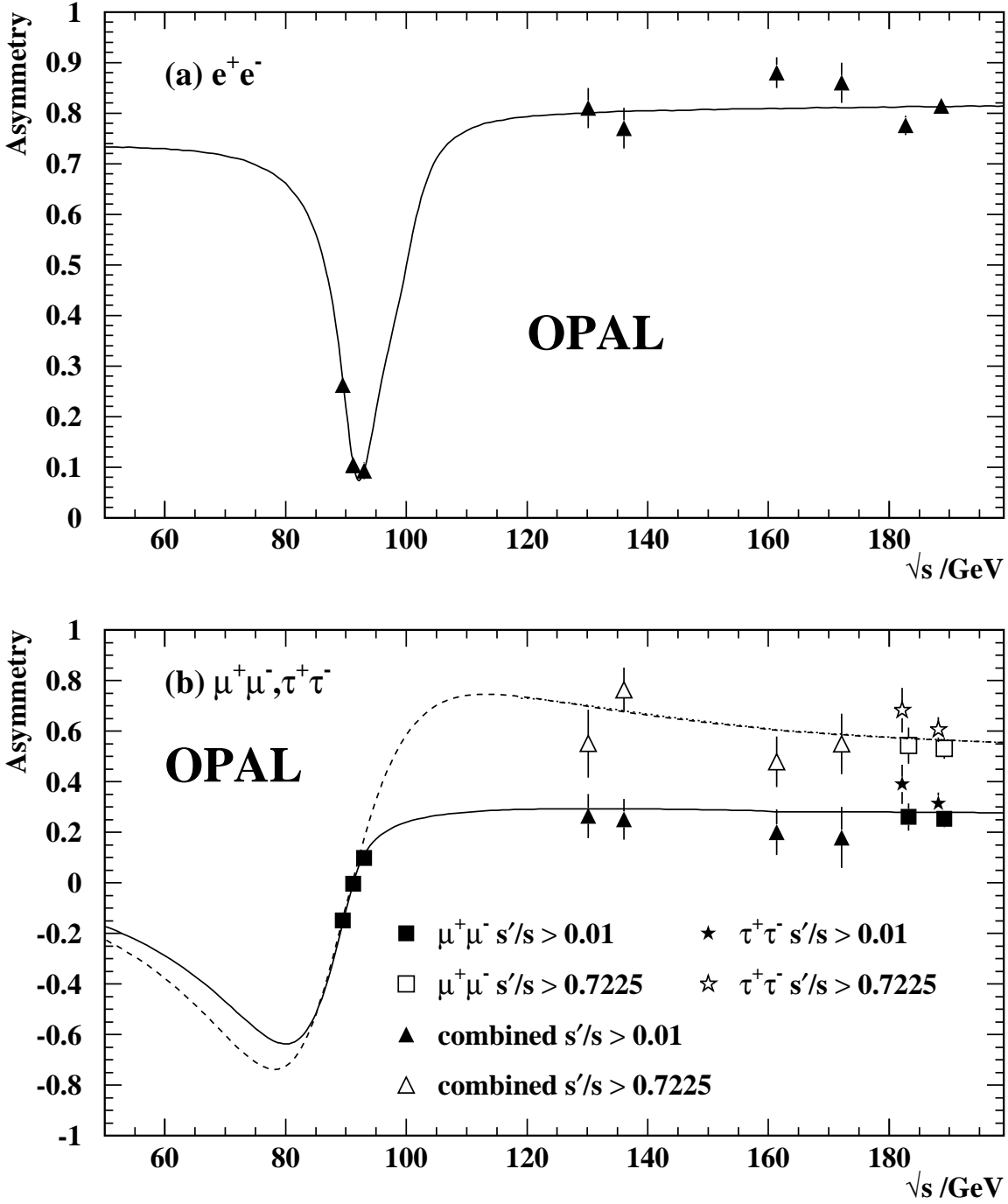
Figure 6: (a) Measured forward-backward asymmetry for electron pairs with $|\cos\theta_{e^-}| < 0.7$ and $\theta_{\text{acol}} < 10°$, as a function of $\sqrt{s}$. The curve shows the prediction of ALIBABA. (b) Measured asymmetries for all ($s'/s > 0.01$) and non-radiative ($s'/s > 0.7225$) samples as functions of $\sqrt{s}$ for $\mu^+\mu^-$ and $\tau^+\tau^-$ events. Some points are plotted at slightly displaced values of $\sqrt{s}$ for clarity. The curves show ZFITTER predictions for $s'/s > 0.01$ (solid) and $s'/s > 0.7225$ (dotted), as well as the Born-level expectation without QED radiative effects (dashed). The expectation for $s'/s > 0.7225$ lies very close to the Born curve, such that it appears indistinguishable on this plot.
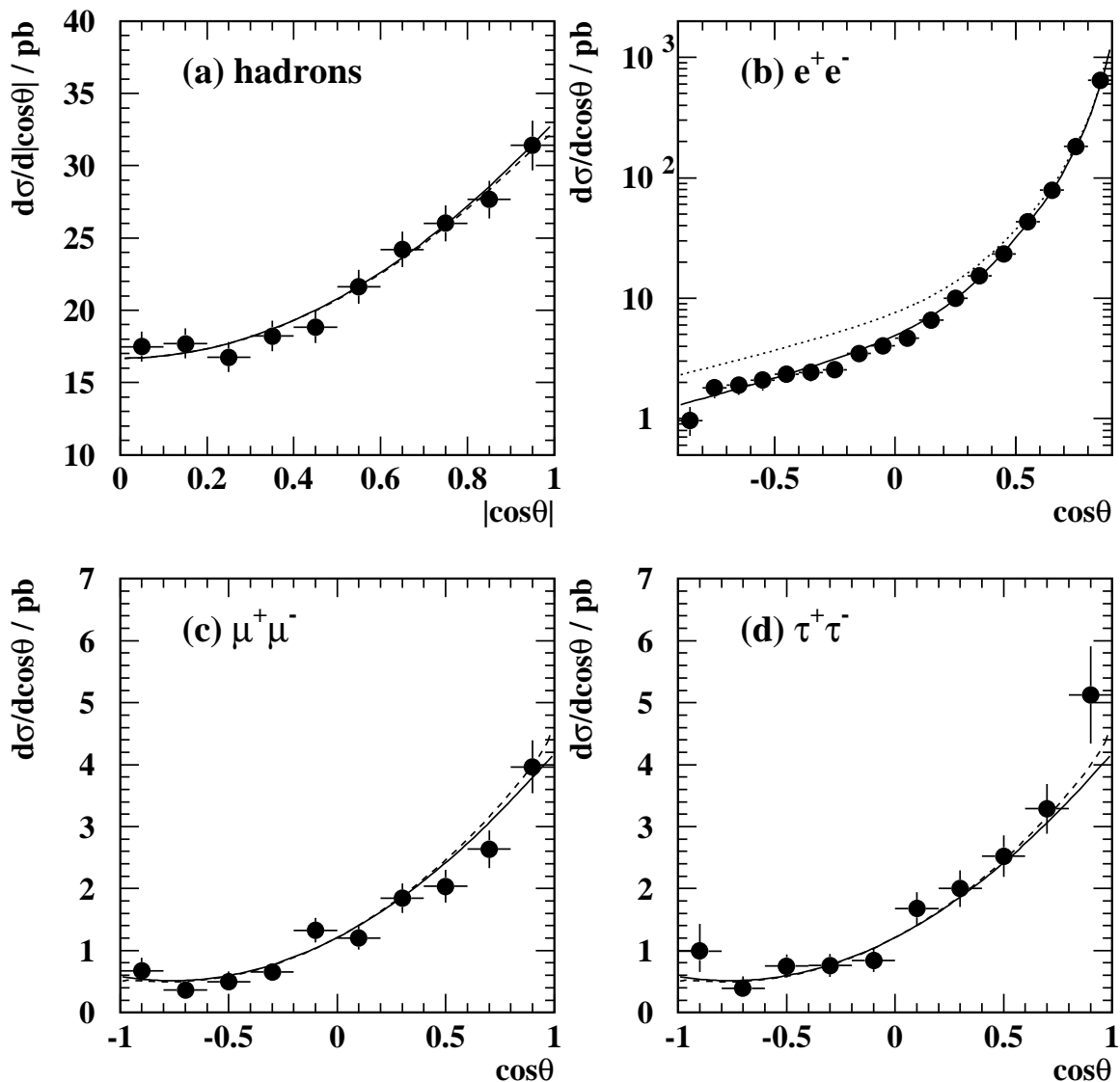
34

OPAL 189 GeV

Figure 7: Angular distributions for (a) hadronic events with $s'/s > 0.7225$, (b) e^+e^- events with $\theta_{\mathrm{acol}} < 10°$, (c) $\mu^+\mu^-$ events with $s'/s > 0.7225$ and (d) $\tau^+\tau^-$ events with $s'/s > 0.7225$. The points show the 189 GeV data, corrected to no interference between initial- and final-state radiation in (a), (c) and (d). The solid curve in (b) shows the prediction of ALIBABA, while the dotted curve shows the prediction with no contribution from t-channel Z exchange. The curves in (a),(c) and (d) show the predictions of ZFITTER with no interference between initial- and final-state radiation (solid) and with interference (dashed).
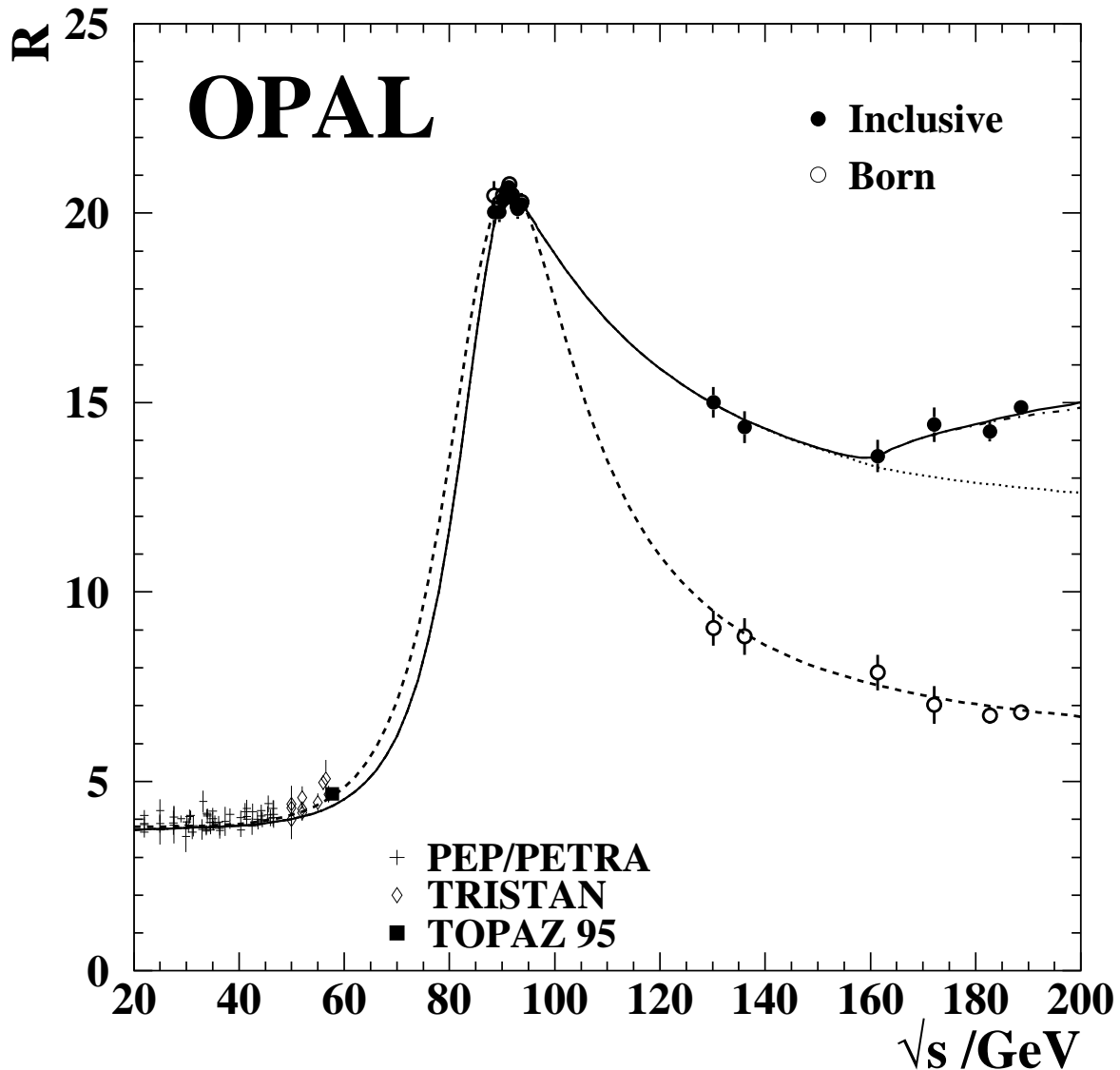
35

Figure 8: Ratio of measured hadronic cross-sections to theoretical muon pair cross-sections as a function of centre-of-mass energy. Values are shown for the inclusive cross-section, $\sigma(q\overline{q}X)$ and for the Born level cross-section. The dotted and dashed curves show the predictions of ZFITTER for these cross-sections, while the solid curve also includes the contributions from W-pairs calculated using GENTLE [34] and from Z-pairs calculated using FERMISV [35]. The dot-dashed curve is the total excluding the Z-pair contribution. Measurements at lower energies are from references [1, 2, 19, 17, 18, 36].
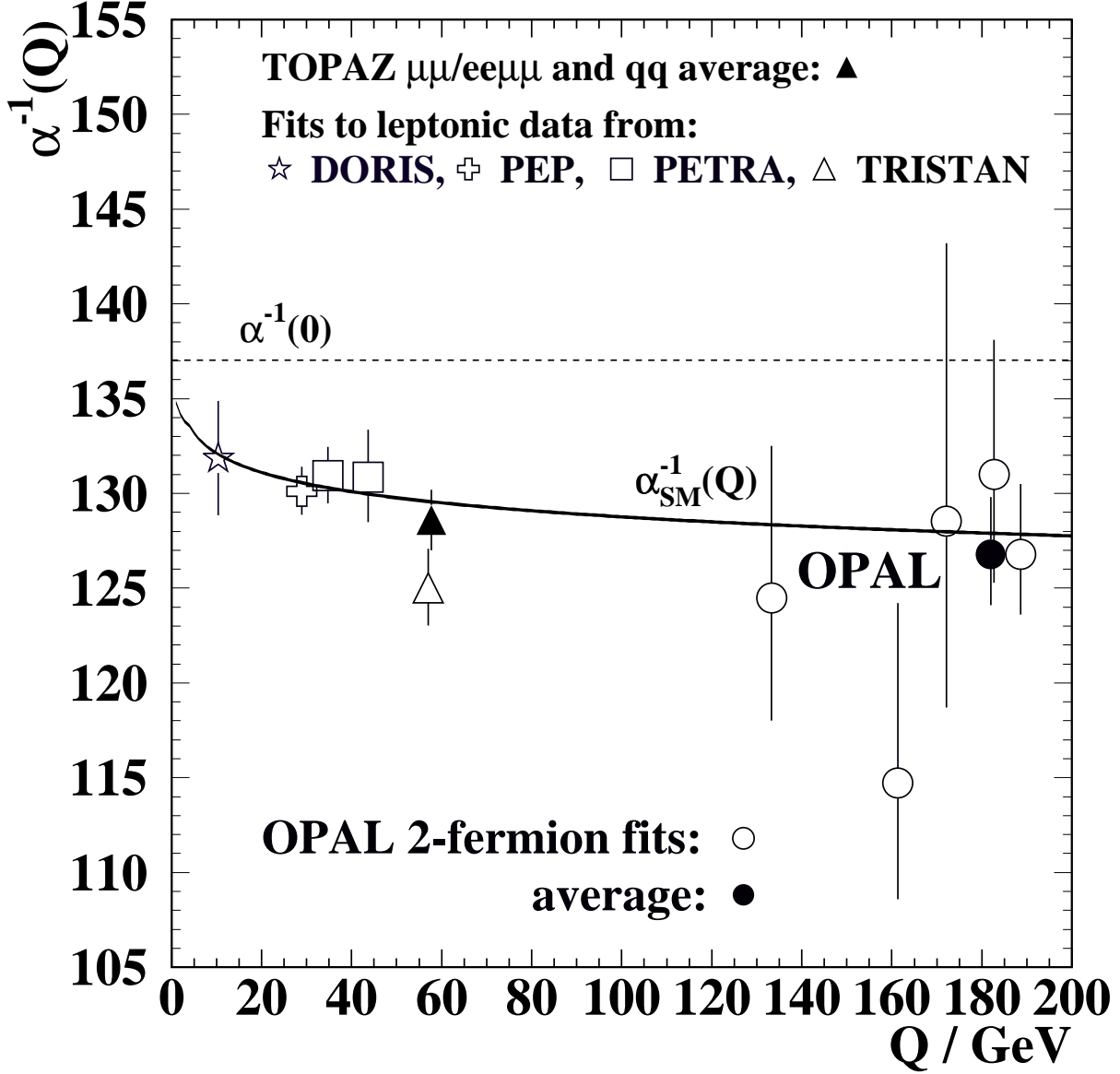
Figure 9: Fitted values of $1/\alpha_{em}$ as a function of Q, which is $\sqrt{s}$ for the OPAL fits. The open circles show the results of fits to OPAL data at each centre-of-mass energy, the closed circle the result of the combined fit in which α_{em} runs with a slope corresponding to its fitted value. The OPAL results at 130–183 GeV are from [2,1]. Values obtained by the TOPAZ experiment [37] and from fits to measurements of leptonic cross-sections and asymmetries at the DORIS, PEP, PETRA and TRISTAN e^+e^- storage rings [38] are also shown. All measurements rely on assuming the Standard Model running of α_{em} up to the Q^2 of the luminosity measurements, $Q_{lumi} \sim 5$ GeV. The solid line shows the Standard Model expectation, with the thickness representing the uncertainty, while the value of $1/\alpha_{em}(0)$ is shown by the dashed line.
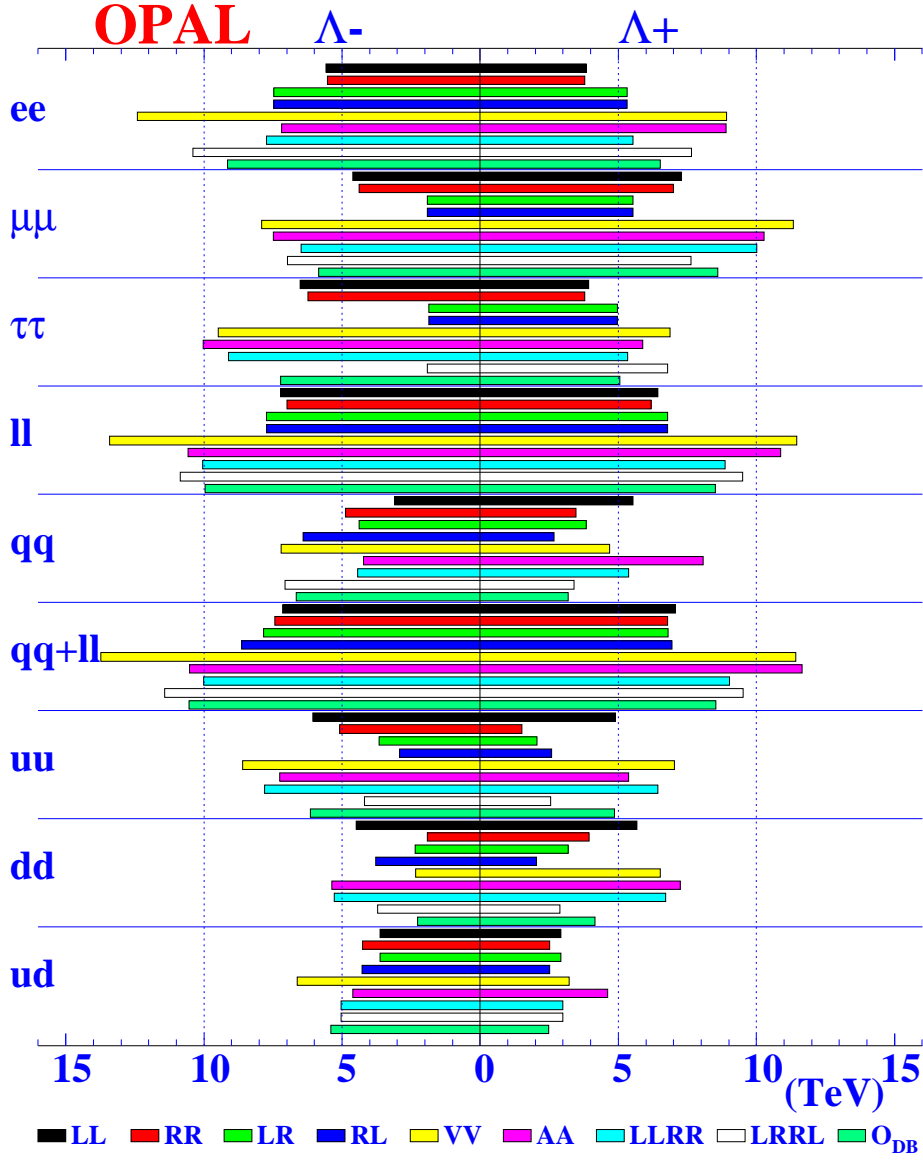
37

Figure 10: 95% confidence level limits on the energy scale Λ resulting from the contact interaction fits. For each channel, the bars from top to bottom indicate the results for models LL to $\overline{\mathcal{O}}_{\mathrm{DB}}$ in the order given in the key.

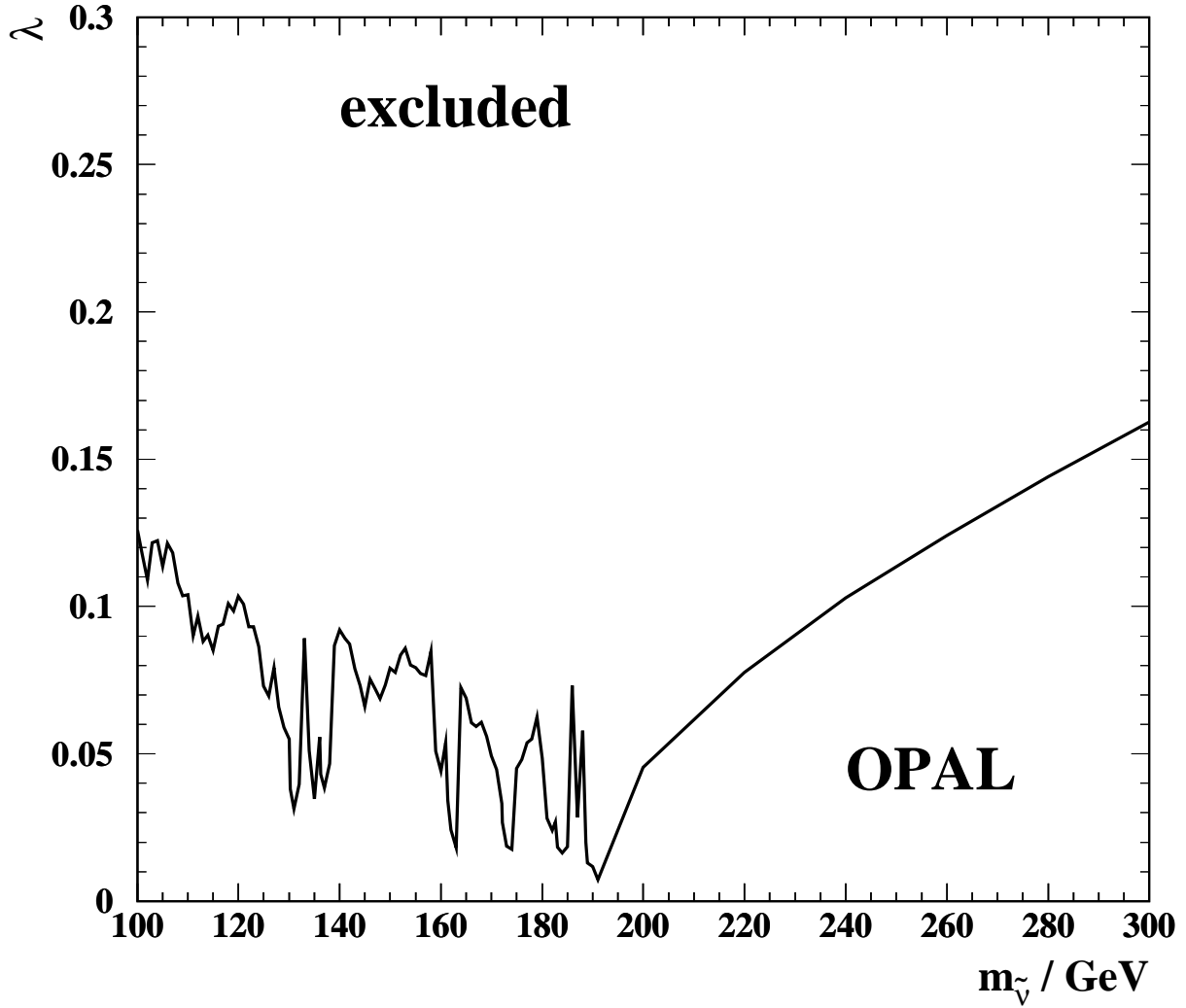**Limits on coupling λ_{131} and λ_{121}**

Figure 11: 95% confidence exclusion limits on λ_{131} (or λ_{121}) as a function of sneutrino mass $m_{\tilde{\nu}}$, derived from e^+e^- s' distributions. The region above the solid line is excluded.
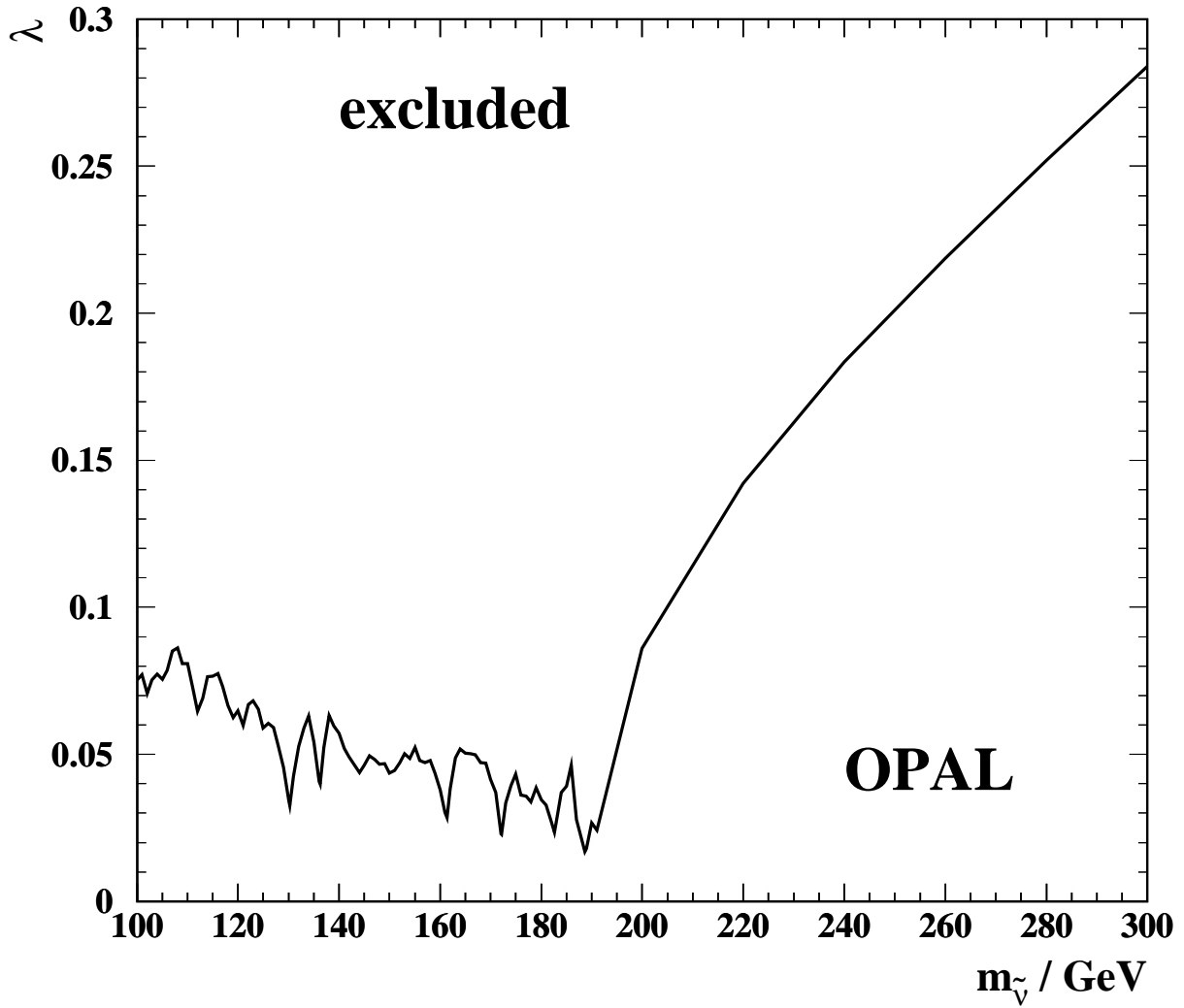
Figure 12: 95% confidence exclusion limit on $\lambda_{131} = \lambda_{232}$ as a function of sneutrino mass $m_{\tilde{\nu}}$, derived from $\mu^+\mu^-$ s' distributions. The region above the solid line is excluded.
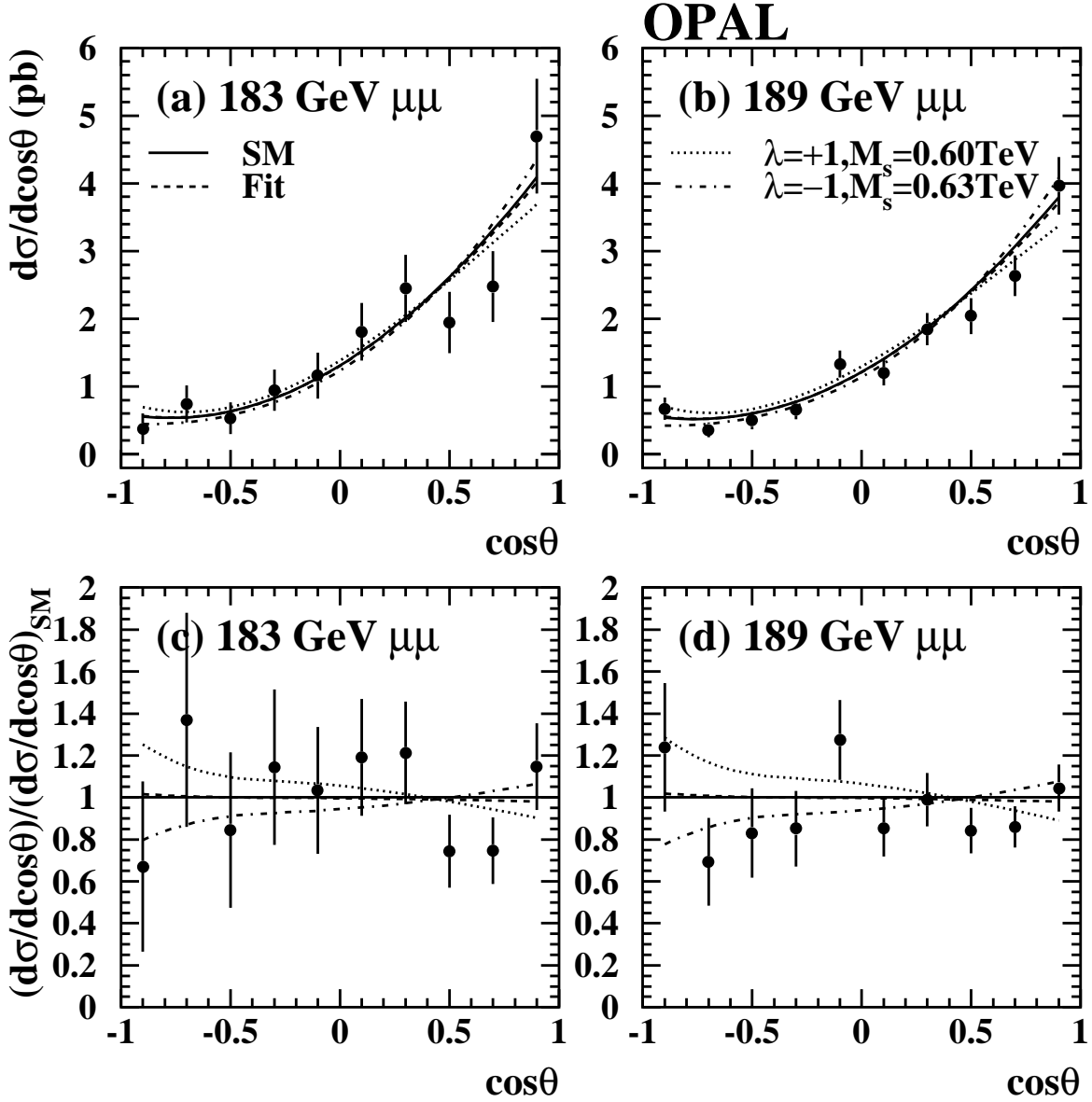
Figure 13: The differential cross-sections for muon pairs at (a) $\sqrt{s} = 183$ GeV and (b) $\sqrt{s} = 189$ GeV. The curves show the Standard Model prediction (solid line), the best fit with the new gravitational interaction (dashed line), and the distributions corresponding to the 95% confidence level limits on M_s with $\lambda = +1$ (dotted line) and $\lambda = -1$ (dot-dashed line). Note that these curves correspond to the simultaneous fit of 183 GeV and 189 GeV data. The ratios of data to Standard Model prediction for (c) 183 GeV muon pairs and (d) 189 GeV muon pairs are also shown.
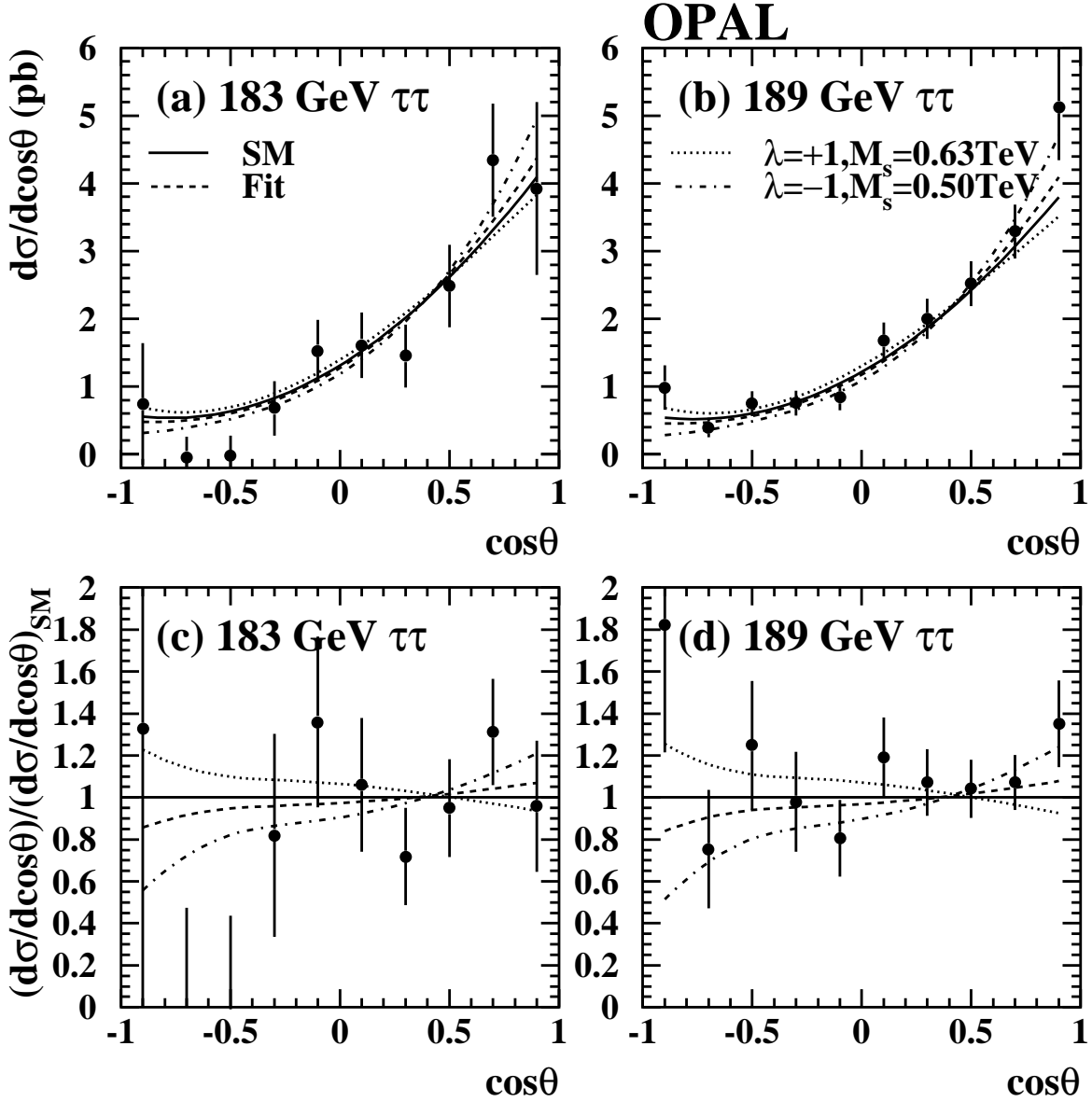
Figure 14: The differential cross-sections for tau pairs at (a) $\sqrt{s} = 183$ GeV and (b) $\sqrt{s} = 189$ GeV. The curves show the Standard Model prediction (solid line), the best fit with the new gravitational interaction (dashed line), and the distributions corresponding to the 95% confidence level limits on M_s with $\lambda = +1$ (dotted line) and $\lambda = -1$ (dot-dashed line). Note that these curves correspond to the simultaneous fit of 183 GeV and 189 GeV data. The ratios of data to Standard Model prediction for (c) 183 GeV tau pairs and (d) 189 GeV tau pairs are also shown.